Charles University in Prague
Faculty of Mathematics and Physics

Master Thesis

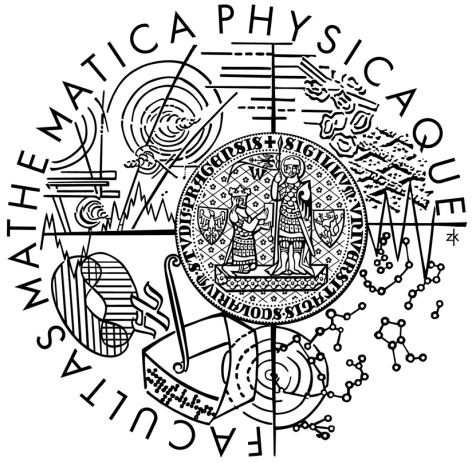

Vojtěch Molda

Flow Simulation Through Multiorifice Using Boltzmann Kinetic Equation

Institute of Theoretical Physics

Supervisor of the Thesis: RNDr. Ing. Jaroslav Hron, Ph.D.

Study Programme: Mathematical and Computer Modeling in Physics and Technique

Prague 2011

Chapter 1

Introduction

1.1 Acknowledgments

It is a pleasure to be able to write this last part of the thesis and thank people who made it possible. It is difficult to overstate gratitude to my wife for carefully preparing such a great working environment for me despite missing me terribly.

I offer my sincerest gratitude to my supervisor Dr. Jaroslav Hron who has supported me whenever I've hit an impasse and has always pointed out with patience and knowledge where the right direction is whilst allowing me the room to work in my own way.

Deepest gratitude are also due to the consultants of the thesis Dr. Tomáš Gronych and Dr. Ladislav Peksa who willingfully provided experimental data and their knowledge and kindness greatly helped in establishind key questions of the thesis.

Lastly I wish to thank my parents. They bore me raised me and supported me all the way up here.

1.2 Solemn Declaration

I declare that I carried out this master thesis independently, and only with the cited sources, literature and other professional sources. I understand that my work relates to the rights and obligations under the Act No. 121/2000 Coll., the Copyright Act, as amended, in particular the fact that the Charles University in Prague has the right to conclude a license agreement on the use of this work as a school work pursuant to Section 60 paragraph 1 of the Copyright Act.

In Prague on August 5^{th} 2011 Vojtěch Molda

1.3 Thesis Assignment

Title: Flow Simulation through Multiorifice using Boltzmann Kinetic Equation
Author: Vojtěch Molda <vojta.molda@gmail.com>
Department: Institute of Theoretical Physics
Supervisor: RNDr. Ing. Jaroslav Hron, Ph.D. <jaroslav.hron@mff.cuni.cz>
Keywords: Rarefied gas, Lattice-Boltzmann method, Boltzmann kinetic equation, Orifice, Computational Fluid Dynamics
Abstract: An attempt to numerically predict flow rate of experimental configuration of orifices in transition between molecular and viscous flow regime is described in detail. Discretization of Boltzmann kinetic equation known as lattice-Boltzmann method is derived and applied unfortunately with very little connection to the original experimental problem due to nearly supersonic nature of the experimental setup. Current quite unsatisfactory state of the art of compressible lattice-Boltzmann method is also presented.

1.4 Contents

Chapter 2

Experimental Motivation

2.1 Dynamic Calibration Procedure for Vacuum Gauges

Calibration process in general comprises a comparison of instrument to be calibrated against absolute indicating instrument of a different kind. Special case of such procedure is measurement of exactly known physical quantity by an instrument to be calibrated. Using already calibrated instrument one can progress further on and calibrate other instruments. It is clear that at the top of the hierarchy there have to be the most precise instrument - primary standard.

Among all the physical quantities there are currently seven that have the privilege of being base units in SI[1] system. Primary standards of all derived quantities must determine the value of measured quantity in terms of base units. Although it can be mediated in several inter-steps.

The pressure can be found of measurements of length, mass and time. Detailed search and analysis show that vacuum gauge whose scale would be possible to determine purely on base units can be constructed down to a range from 1 Pa to 10^{-2} Pa depending on the required precision.

To calibrate gauges for lower pressures the fact that one can establish exactly known value of pressure by a thermodynamic process done with a certain amount of gas is exploited. For instance the thermodynamic process can be a static expansion of gas from smaller into larger reservoir. The initial pressure can measured by the gauges related to the base units. The pressure after the expansion process can be calculated by Boyle's law. This way the lower bound of the pressure range that can be determined in base units can be extended. Although detail investigation shows that such procedure can't be extend infinitely as one hits technological and physical obstacles.

Dynamic methods rather than using statically stepwise increase of volume rely on steady flow of gas expanding continuously throughout the vacuum system. As depicted in Figure 2.1 gas flows from the upstream chamber via orifice to the downstream chamber and from there finally towards pump. The orifice typically consist of a circular hole in a thin plate. Pressure p_1 in the upstream chamber is measured by a reference calibrating gauge and pressure p_0 in the downstream chamber is determined from a gauge to be calibrated.

[1] SI is abbreviation of International Unit System in French (Le Système International d'Unité)

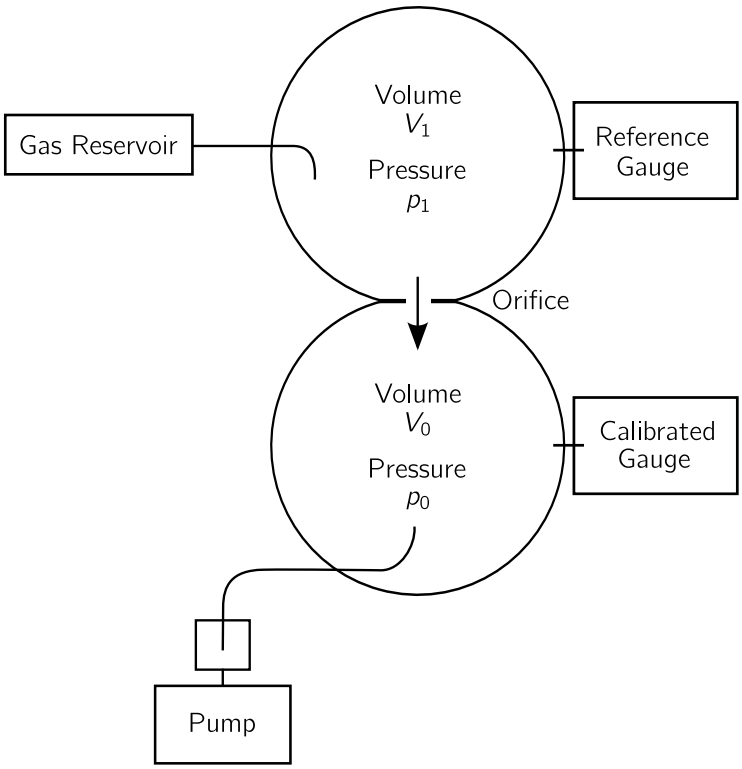

Figure 2.1: Dynamic Calibration Procedure Schematics

The relation between pressures p_1 and p_0 could be determined in a following way. If we take conservation of mass for both chambers and integrate it over their individual volumes V_1 and V_0 then using Gauß theorem yields

$$\int_{V_1} \partial_t \rho_1 dV_1 + \oint_{\partial V_1} \rho_1 \mathbf{v} \cdot \mathbf{dA_1} = 0, \tag{2.1}$$

$$\int_{V_0} \partial_t \rho_0 dV_0 + \oint_{\partial V_0} \rho_0 \mathbf{v} \cdot \mathbf{dA_0} = 0. \tag{2.2}$$

Vector $\mathbf{v} = \mathbf{v}(\mathbf{x}, t)$ denotes gas flow velocity field in both volumes. $\rho_1 = \rho_1(\mathbf{x}, t)$ and $\rho_0 = \rho_0(\mathbf{x}, t)$ are density fields in upstream and downstream chamber of the apparatus. Density in up and downstream chamber ρ_1 and ρ_0 can be written using pressures p_1, p_0 utilizing the equations

$$p_1 = \frac{k\Theta}{m}\rho_1, \tag{2.3}$$

$$p_0 = \frac{k\Theta}{m}\rho_0. \tag{2.4}$$

m denotes mass of atoms or molecules of the flowing gas and k denotes Boltzmann constant. We assume that temperature Θ is constant and doesn't change over time. Pressures

p_1, p_0 are constants only in space. Equations (2.1), (2.2) could be simplified to (2.5) and (2.6). It would be tempting to cancel out the factor preceding the brackets. As will become clear later this would change the physical units of the equation which is undesired effect.

$$\frac{m}{k\Theta}\left[V_1\partial_t p_1 + p_1 \oint_{\partial V_1} \mathbf{v}\cdot\mathbf{dA}\right] = 0 \tag{2.5}$$

$$\frac{m}{k\Theta}\left[V_0\partial_t p_0 + p_0 \oint_{\partial V_0} \mathbf{v}\cdot\mathbf{dA}\right] = 0 \tag{2.6}$$

We take into consideration impenetrable walls represented by boundary condition $\mathbf{v}\cdot\mathbf{dA} = 0$. It holds everywhere except for orifice, pump inputs and gas reservoir outlet. Substitution of boundary condition to the surface integral breaks it into three pieces. One represents flow across the area of the gas reservoir outlet $\mathbf{A_1}$. Second is flow through cross section of the orifice $\mathbf{A}$ and third is integration over the surface of the inlet of the vacuum pump $\mathbf{A_0}$. If we introduce mean gas velocity across a planar surface $\langle\mathbf{v}\rangle_{\mathbf{X}} = \frac{1}{|\mathbf{X}|}\int_{\mathbf{X}}\mathbf{v}dX$. $\mathbf{X}$ denotes vector normal to the surface. The magnitude of $\mathbf{X}$ is equal to the area of the surface. Equations (2.5), (2.6) can be written as

$$\frac{m}{k\Theta}\left[V_1\partial_t p_1 + p_1\left(\langle\mathbf{v}\rangle_{\mathbf{A_1}}\cdot\mathbf{A_1} + \langle\mathbf{v}\rangle_{\mathbf{A}}\cdot\mathbf{A}\right)\right] = 0, \tag{2.7}$$

$$\frac{m}{k\Theta}\left[V_0\partial_t p_0 + p_0\left(\langle\mathbf{v}\rangle_{\mathbf{A_0}}\cdot\mathbf{A_0} - \langle\mathbf{v}\rangle_{\mathbf{A}}\cdot\mathbf{A}\right)\right] = 0. \tag{2.8}$$

Since pumping speed of the vacuum pump is very large compared to the throughput through the orifice first term in equation (2.8) disappears since pressure in the downstream chamber is not changing in time. If we sum the equations (2.7) and (2.8) we arrive at equation (2.9) expressing the dependence of pressure p_1 on time and other factors.

$$\underbrace{\frac{m}{k\Theta}V_1}_{\widetilde{V}_1}\partial_t p_1 + (p_1 - p_0)\underbrace{\frac{m}{k\Theta}\langle\mathbf{v}\rangle_{\mathbf{A}}\mathbf{A}}_{K} = \underbrace{-\frac{m}{k\Theta}\left(p_1\langle\mathbf{v}\rangle_{\mathbf{A_1}}\cdot\mathbf{A_1} + p_0\langle\mathbf{v}\rangle_{\mathbf{A_0}}\cdot\mathbf{A_0}\right)}_{M} \tag{2.9}$$

Meaning of the first term on the left side of equation (2.9) is obvious. It expresses rate of change of pressure over time multiplied by some factor depending on the type of gas, volume and temperature.

Second term consists of difference between pressures in the upstream and downstream chambers p_1 and p_0 multiplied by the cross section of the orifice and mean gas velocity. It can be thought as throughput through the orifice. Omitting the pressure difference this term will be denoted as conductivity K of the orifice.

Right side of the equation evaluates mass flow rate through the vacuum system and will be denoted as M. Final differential equation describing development of pressure in the upstream chamber over time is (2.10).

$$\widetilde{V_1}\partial_t p_1 + K(p_1 - p_0) = M \tag{2.10}$$

Constant K could be determined experimentally by closing valves bridging the upstream chamber with gas reservoir. Since pressure p_0 is several orders of magnitude smaller than p_1 it could be neglected for the purpose of determination of the time development of the pressure in the upstream chamber. If the pressure p_0 wouldn't be significantly smaller this fairly complicated calibration procedure being described here would be deemed absolutely unnecessary since direct methods could be used to calibrate the gauge. If the valve in gas reservoir is closed then mass flow rate $M = 0$. Solution of simplified ordinary differential equation (2.10) under assumptions stated above is

$$p_1(t) = p_1(t_0) \exp\left(-\frac{K}{\widetilde{V_1}}(t - t_0)\right). \tag{2.11}$$

By fitting the experimental data recorded by the reference gauge in the upstream chamber to the equation (2.11) one easily determines the value of K.

Vacuum system is in quasi-stationary state during calibration process. Pressure p_1 is varied extremely slowly and thereby term evaluating time derivative of pressure in (2.10) can be neglected. Under this assumption we arrive at simplified and practically used equation for mass flow rate of orifice

$$K(p_1 - p_0) = M. \tag{2.12}$$

Relation (2.12) is an analogy to Ohm's law. Mass flow rate M is equal to conductivity times difference in pressure. Mass flow rate is a metaphor of electrical current. Conductivity is inverse of resistance and difference in pressure is analogous to a voltage drop.

Schematics displaying the detail and dimensions of the orifice that is separating the volumes V_0 and V_1 is on Figure 2.2.

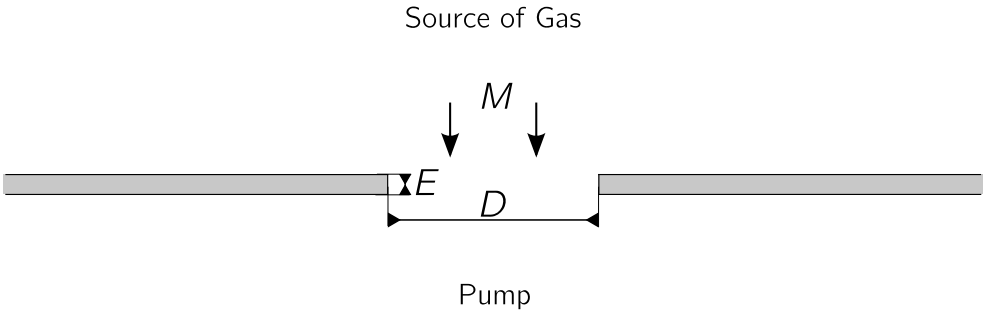

Figure 2.2: Orifice

It is worth noting that other more sophisticated shapes of duct than one presented here are also used. For instance one can form an orifice by making a spherically or conically shaped duct. Reason for such shapes is that the created domain allows analytical solutions of fluid dynamics equations can which in turn allows easy theoretical mass flow predictions.

Bird in [6] states that in molecular regime the mass flow rate of infinitely thin orifice of diameter D from pressure p_1 into vacuum can be evaluated analytically as

$$\sqrt{\frac{\pi\gamma}{2}}\left(\frac{D}{2}\right)^2\frac{p_1}{c}=M_0. \tag{2.13}$$

Specific heat capacity is denoted as γ and adiabatic speed of sound is denoted as c and determined from

$$c=\sqrt{\gamma\frac{k\Theta}{m}}. \tag{2.14}$$

Speed of sound depends only on the type of gas by means of specific heat capacity γ, molecular mass m and temperature θ.

We introduce reduced mass flow rate r used further on. It is defined in (2.15) as ratio of actual mass flow rate M divided by flow rate in molecular regime M_0

$$r=\frac{M}{M_0}. \tag{2.15}$$

Now it becomes clear that if we would have canceled out the term $\frac{m}{k\Theta}$ a few steps above the reduced mass flow rate wouldn't be dimensionless. Units of r would be J/kg. The reason is that canceling of the $\frac{m}{k\Theta}$ factor would yield R in J/s rather than kg/s. Different unit doesn't pose a problem since both views are equivalent and they differ only by a multiplicative constant but a reasonable definition of reduced flow rate should be dimensionless.

According to Berman [4] reduced flow rate needs to be modified by factor ξ adjusting for finite thickness of the orifice plate $\xi = E/D$. The orifice thickness E is assumed to be much smaller than the diameter $E \ll D$.

$$r=\frac{M}{M_0}(1-\xi) \tag{2.16}$$

2.2 Limitations of Dynamic Calibration Procedure

It is clear from derivation presented in previous section that there exist severe limitations. Dynamic calibration methods require numerous theoretical propositions. Assumption about constant pressures and temperatures in the vacuum system could be summed up into single premise. Whole system must be in thermodynamic equilibrium state which in other words means that particles must obey Maxwell distribution of velocities.

Serious problem is that such a statement is obvious contradiction whereas the gas flows from one chamber to the other and expands on the way. Thus it is more realistic to assume sort of quasi-statical thermodynamic equilibrium. Maxwell distribution is distorted only to a small degree and the distortion is localized in very small area surrounding the orifice. To what extent is such assumption valid depends on character of flow. It is worth noting that compliance rate of quasi-statical equilibrium assumption determines the degree of linearity of (2.12).

For the quantification of the nature of the flow it is common practice to introduce Knudsen number Kn (2.17). It is defined as ratio of mean free path of molecules $\langle\lambda\rangle$ and characteristic dimension of the studied system $\overline{x}$. We consistently use orifice diameter D as characteristic dimension throughout the thesis.

$$Kn = \frac{\langle\lambda\rangle}{\overline{x}} = \frac{\langle\lambda\rangle}{D} \tag{2.17}$$

Evaluation of mean free path is somewhat cumbersome. There is classical kinetic theory result for hard sphere molecules where mean free path can be expressed as a function of among other things molecular diameter d. Such a relation offers very little practical use considering it is nearly impossible to accurately determine correct value of d. Hard sphere model isn't arguably the most accurate description of molecular interaction and so are many other available kinetic theory models. A vague parameter of this kind in the heart of the definition of the main scaling parameter is highly inappropriate. To address the issue we adopt approach presented by Zhang in [48] where we consider the mean free path defined as a function of only macroscopic variables. Namely the variables are kinematic viscosity μ, sound speed c and pressure p

$$\langle\lambda\rangle = \sqrt{\frac{\pi}{2\gamma}}\frac{\mu c}{p}. \tag{2.18}$$

For Knudsen number higher than approximately 1 the flow happens under molecular regime. Individual molecules of gas are passing through the orifice almost without interactions. In molecular regime relation (2.12) remains linear and mass flow rate is proportional to the difference in pressure.

As the Knudsen number decreases below 1 number of collisions taking place on a characteristic length scale increases and behavior of gas molecules begin to change. Density becomes high enough that particles going in particular direction collide with their neighbors and propel them in the direction of their motion. Kind of a group motion takes place in gas. Such phenomenon is called viscosity of fluids. This effect causes deviation from linear behavior of mass flow rate M. It is no longer linearly dependent on the pressure difference and (2.12) becomes inaccurate.

In viscous regime throughput through the orifice increases due to viscosity effects and equation (2.12) is no longer linear in pressure difference. The transition happens in the range of Knudsen number between 1 and 10^{-3}. Since pressure is proportional to inverse of mean free path $\langle\lambda\rangle$ relations (2.17) and (2.18) effectively limit diameter of the orifice D which is necessary to maintain molecular character of the flow.

Throughput through the orifice is proportional to D^2 and thereby decreases steeply with the diameter. From experimental point of view the procedure lacks required precision if the throughput gets too small. The reason behind it is that the measurement of flow rate from the gas reservoir is less accurate for smaller throughput. One of the main issues in vacuum equipment - out-gassing of walls makes things even worse. Inner surface of the vacuum system even if properly treated is capable of adsorbing and later releasing significant amount of gas. This in turn creates inner flows that distort measurements.

To overcome such a limitation one can arrange several small orifices next to each other in order to increase throughput. Such assembly of orifices forms so-called multiorifice. Beside the obvious increase in precision of flow rate measurement one gets further benefits. It is easy to see that if relative accuracy of determination of diameter D remains the same the overall accuracy decreases with increasing number of holes as $1/\sqrt{n}$.

2.3 Multiorifice Experiment

Arrangement of multiorifice brings several interesting questions. Dynamic calibration procedure that is extensible to higher pressures would require to lay huge amount of orifices as small as up to date manufacturing processes allow very close to each other. The question is how to determine the spacing of orifices so they wouldn't influence each other. The overall conductivity could in that case be calculated as simple sum of linear relations (2.12).

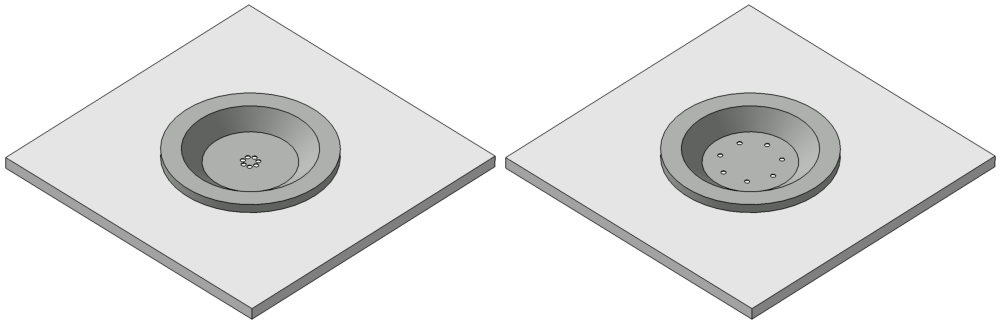

Figure 2.3: Multiorifice Setup

There has been an experiment studying multiorifices conducted by Dr. Tomáš Gronych, Dr. Ladislav Peksa and Dr. Martin Jeřáb. All are members of the Vacuum group at Department of Surface and Plasma Science, Faculty of Mathematics and Physics, Charles University in Prague. Aim of the experiment was to measure how spacing of orifices influences the mass flow rate M.

The multiorifice was setup as depicted on Figure 2.3. Argon gas was forced by pressure gradients to flow through an obstacle presented by the multiorifice. Each multiorifice consisted of 7 circular holes of diameter $D = 0.4\ mm$. Centers of the holes were placed in corners of a regular heptagon. Measurement was done on several multiorifices that differed in the length of the edge of heptagon F. Dimensions of the multiorifice are shown in Figure 2.4. The values of F were chosen to be $\{0.1,\ 0.2,\ 0.3,\ 0.4,\ 0.6,\ 0.8,\ 1.1,\ 1.6\}\ mm$. To get a clearer picture two extreme cases are displayed on Figure 2.3.

In order to get a direct comparison the measurements were also done on a single circular orifice as is shown on Figure 2.5. The diameter of single orifice was chosen to be $D_0 = 1.027\ mm \approx \sqrt{7}D$ to maintain the same overall area.

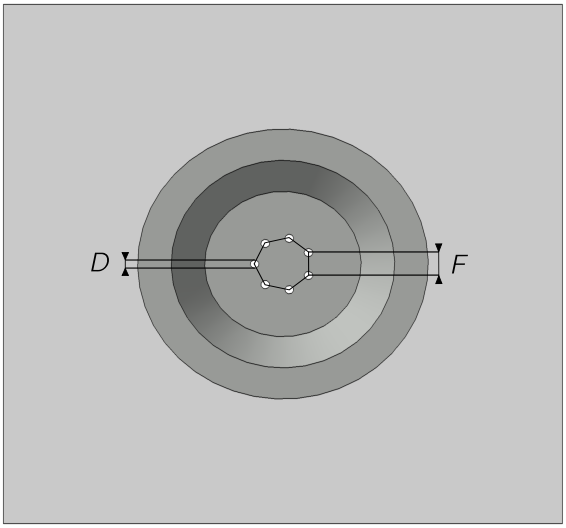

Figure 2.4: Multiorifice Dimensions

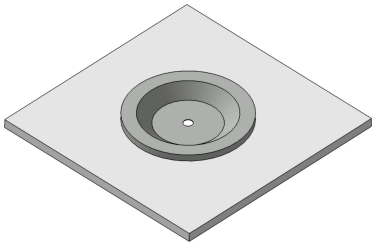

Figure 2.5: Single orifice

Multiorifices were manufactured by laser drilling of the tantalum foil. The thickness of the foil was $E = 0.015\ mm$. This gives ratios of thickness to diameter of the orifice $\xi = 0.0375$ and $\xi_0 = 0.0146$ for the single orifice case.

As was exploited in aforementioned derivations the pressure p_0 downstream the orifice was maintained significantly smaller than the driving pressure p_1 upstream the orifice. In fact the ratio of pressures always fulfilled $p_1/p_0 > 1000$. The whole experimental apparatus was moved to basement in order to hold a constant temperature $\theta = 299\ K$ during the experiment.

The experimental dependence of reduced mass flux r on Knudsen number is shown in Figure 2.6. There are certain unexpected discontinuities at some points in the data. This is caused by the necessity to use three different vacuum gauges to cover required pressure range. From the experimental data it can be roughly estimated that orifices that are spaced more than $3 - 4$ diameters apart have negligible effects on their neighbors.

As is shown later in chapter 4.5 another dimensionless parameter responsible for the scaling is Mach number Ma. It is defined as ratio of characteristic macroscopic flow speed $\overline{v}$ and speed of sound c

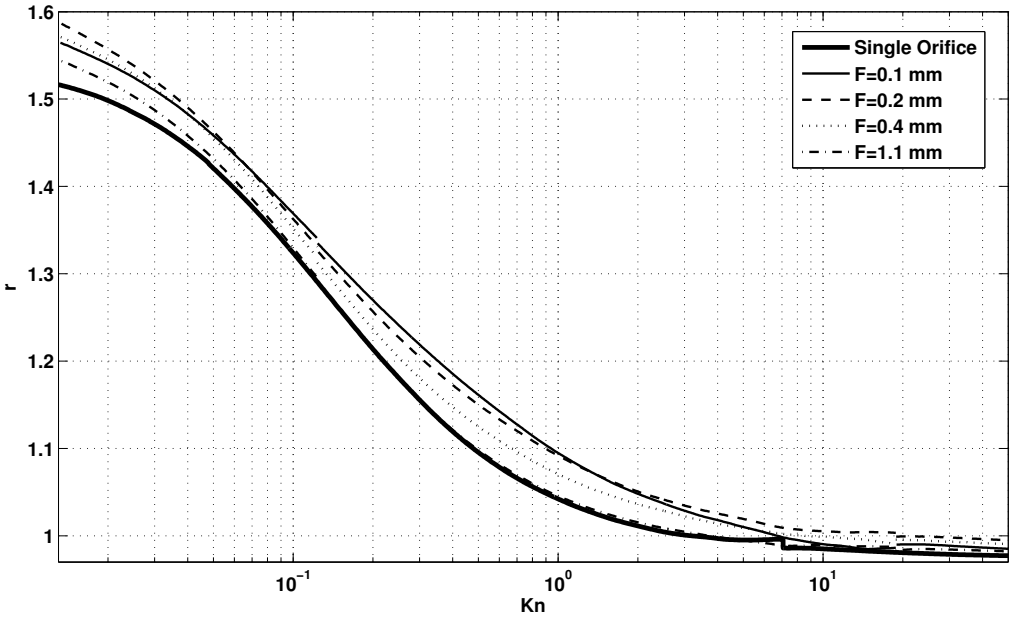

Figure 2.6: Measured Experimental Dependence of Reduced mass flow on Knudsen number for different configurations of multiorifice

$$Ma = \frac{\overline{v}}{c}. \tag{2.19}$$

Characteristic velocity $\overline{v}$ is chosen to be the average component of the velocity normal to the cross section of the orifice

$$\overline{v} = \frac{\langle \mathbf{v} \rangle_{\mathbf{A}} \cdot \mathbf{A}}{|\mathbf{A}|}.$$

The reason of this choice is that value of $\overline{v}$ can be easily evaluated from the experimental value of mass flow rate $R = \rho_1 \langle \mathbf{v} \rangle_{\mathbf{A}} \cdot \mathbf{A}$. Range of parameters that needs to be investigated for each multiorifice configuration is displayed on Figure 2.7.

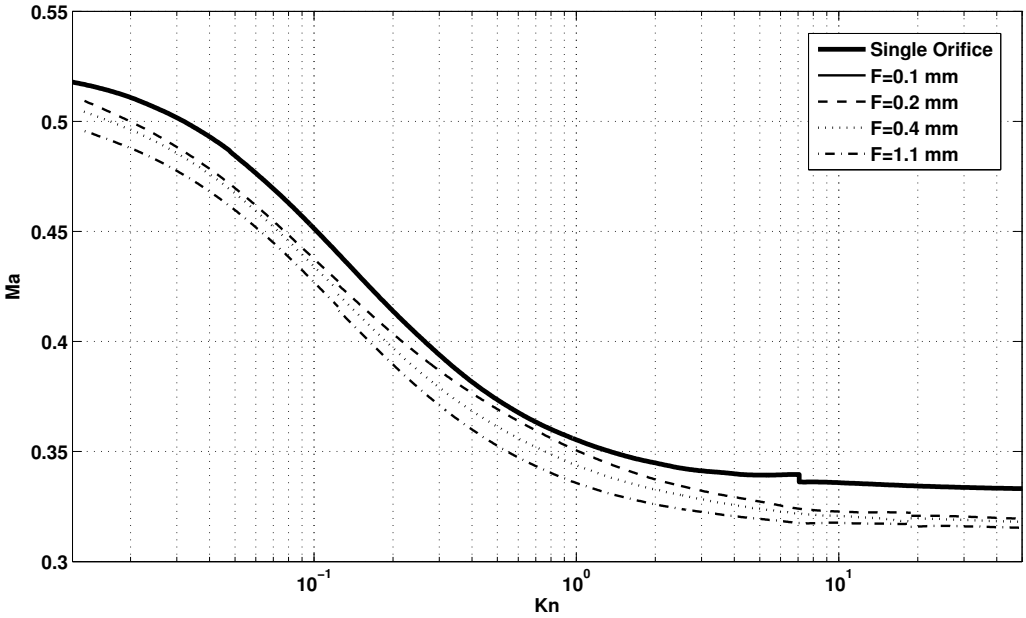

Figure 2.7: Range of Mach number and Knudsen number for Different Configurations of Multiorifice

Chapter 3

Theoretical approaches

3.1 Navier-Stokes Equations

First choice when it comes to fluid dynamics is system of Navier-Stokes equations (3.1),(3.2) and (3.3). We denote density of body forces as $\mathbf{f}$, stress tensor as $\mathbb{T}$, energy density as e, density of heat sources as q and vector of heat flux as $\mathbf{q}$. System of Navier-Stokes equations express conservation of macroscopic properties as stated by Newton's second law. However there are some difficulties in solving them for the purpose of simulation of rarefied gas flow.

$$\partial_t \rho + \nabla \cdot (\rho \mathbf{v}) = 0 \tag{3.1}$$

$$\partial_t (\rho \mathbf{v}) + \nabla \cdot (\mathbf{v} \otimes \mathbf{v}) = \mathbf{f} + \nabla \cdot \mathbb{T} \tag{3.2}$$

$$\partial_t e + \nabla \cdot (e\mathbf{v}) = \mathbf{f} \cdot \mathbf{v} + \nabla \cdot (\mathbb{T}\mathbf{v}) + q - \nabla \cdot \mathbf{q} \tag{3.3}$$

Continuum description is valid as long as the smallest significant volume in the flow contains a number of molecules large enough to establish averages. Specifically the Navier-Stokes equations fail when gradients of macroscopic variables become so steep that their scale is of the same order as mean free path of the molecules of fluid. Such a failure is typically encountered when studying the inner structure of a shock wave or boundary layer effects. In other words Knudsen number is required to be several orders of magnitude smaller than one.

Link between the macroscopic and microscopic quantities means that equations expressing conservation laws may be derived using either continuum or molecular approach. This might suggest that none of the approaches could provide us with information that is not available to the other. It must be remembered that conservation laws do not provide a complete set unless constitutive relations are added. Constitutive relations express stress tensor $\mathbb{T}$ and heat flux $\mathbf{q}$ as a function of other macroscopic variables. Even if the constitutive relations would be acceptably accurate the most problematic portion of them is the dependence of kinematic viscosity ν on Knudsen number Kn. Qualitative character of this relation is depicted on Figure 3.1. For low pressures viscosity is nearly zero as almost no collisions occur in gas. In higher pressures viscosity reaches limit denoted as ν_{NS}. The value of ν_{NS} is viscosity of the given gas as we commonly understand it under standard atmospheric conditions. It is very difficult if

not impossible to measure the relation experimentally and we would require it as data for the solution.

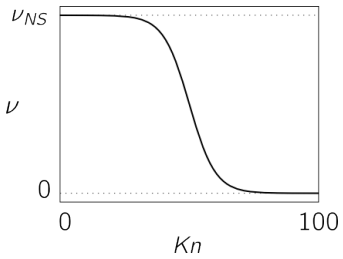

Figure 3.1: Qualitative dependence of viscosity on Knudsen number

However it is failure of completing the system that limits the range of validity of the continuum equations more seriously rather than uncertain determination of viscosity.

It seems so there is no alternative other than Boltzmann kinetic equation when Knudsen number is of order unity or larger. It is worth noting that there are two ways in achieving large Knudsen numbers.

In rarefied gases density of particles is very small and therefore mean free can reach very high values as is the case in this thesis. Other possibility is to decrease characteristic dimension of the system. This is the case in some MEMS[1] devices like yaw rate sensors or accelerometers. Flow in MEMS devices happens in microchannels[2] layered on a silicon substrate. As the development of such devices accelerates increasing number of industrial problems require deep understanding of high Knudsen number flows.

3.2 Boltzmann Kinetic Equation

The kinetic theory of gases pioneered by Ludwig Boltzmann at the second half of the 19^{th} century provides description at the scale between traditional hydrodynamic Navier-Stokes equations and atomistic approach. Hydrodynamic equations don't allow to capture physical phenomena that significantly deviates from thermodynamic equilibrium.

Atomic approach on the other hand suffers from large number of variables required for proper description. It is possible to develop simplified simulation methods capable of delivering results on up to date computers. DSMC[3] method proposed by Bird in [6, 7] is the most popular amongst many researchers in the field of rarefied gas dynamics. There exists numerous modifications of the original method which are suited for particular problem of interest. Simulation methods suffer severe criticism for their non-mathematical foundation. Lack of mathematical rigor provides very poor connection to the solution of Navier-Stokes or Euler equations. Due to the physical and stochastic basis the DSMC method the existence, uniqueness and convergence

[1] Micro Electro-Mechanical System

[2] At the date of writing thesis as small as 10^{-9} m.

[3] Direct Simulation Monte Carlo

questions that are of significant importance in traditional mathematical analysis are considered unimportant.

It is necessary to point out that the derivation of the Boltzmann kinetic equation itself is not straightforward and proposition free as it may seem. Discovery of a new physical law will always require more intuition than rigor.

The chain of reasoning employing the Liouville operator and kinetic theory assumptions about molecular chaos and non-correlated binary collisions presented in [35, 12, 11] are not essentially different from assumptions behind the DSMC method. In fact DSMC is advantageous in some cases of chemically reacting flows with ternary reactions since it doesn't rely on existence of inverse collisions.

As is in detail described in [46, 34, 8] numerical solution of Boltzmann kinetic equation was originally developed on the basis of lattice-gas cellular automaton and their continuous successor lattice-Boltzmann method. Nowadays these methods of solving gas kinetics can be viewed as a very specialized and mathematically rigorous way of discretizing the Boltzmann kinetic equation as will be shown later.

Chapter 4

Boltzmann Kinetic Equation

4.1 Basic Properties of the Boltzmann Kinetic Equation

The state of the gas in the Boltzmann kinetic equation is determined by a distribution function $f = f(\mathbf{x}, \mathbf{u}, t)$. Arguments of f come from the phase space which consists of both macroscopic variables. The position vector $\mathbf{x} \in \Omega$ and microscopic velocity $\mathbf{u} \in \mathbb{R}^3$. Domain occupied by gas Ω is a subset of $\mathbb{R}^3$ with a reasonable boundary. Generally the Boltzmann kinetic equation can be written in an arbitrary number of spatial dimensions but since it is typically used in 3D we will limit ourselves to this case. However 1D or 2D cases are not substantially different and results valid for 3D apply as well for them[1].

The distribution function f represents density in an infinitesimal phase space volume. Mass of a small cube of size dx by du around point $(\mathbf{x}, \mathbf{u})$ at time t can be approximated by $f(\mathbf{x}, \mathbf{u}, t)\ dx^3 du^3$. From this it easily follows that physical unit of distribution function f is $kg \cdot m^{-3} \cdot (m/s)^{-3}$. The distribution function is always positive in order to avoid negative density.

The function f itself isn't directly observable in a similar fashion as wave function in quantum mechanics. All measurable macroscopic quantities can be expressed in terms of microscopic averages over the whole velocity part of the phase space. The local density ρ, velocity $\mathbf{v}$, pressure tensor $\mathbb{P}$ and energy density e are calculated as moments of f

[1] There are 4D relativistic versions of the Boltzmann equation that are typically used to describe early stages of the universe or plasma dynamics. Relativistic Boltzmann equation differs in many aspects and the approach presented here doesn't apply to it.

$$\rho = \int_{\mathbb{R}^3} f(\mathbf{x}, \mathbf{u}, t)\, du^3, \tag{4.1}$$

$$\rho\mathbf{v} = \int_{\mathbb{R}^3} \mathbf{u}\, f(\mathbf{x}, \mathbf{u}, t)\, du^3, \tag{4.2}$$

$$\rho\mathbb{P} = \int_{\mathbb{R}^3} \mathbf{u} \otimes \mathbf{u}\, f(\mathbf{x}, \mathbf{u}, t)\, du^3, \tag{4.3}$$

$$\rho e = \int_{\mathbb{R}^3} \mathbf{u^2}\, f(\mathbf{x}, \mathbf{u}, t)\, du^3. \tag{4.4}$$

It is possible in a mathematically very rigorous way as was shown by Cercignani in [12, 13] to start from Newton's laws and deduce whole hierarchy of models consisting of linear partial differential equations. The deduction of hierarchy is based on scaling known as the Boltzmann-Grad limit. The number of molecules N is let to infinity and at the same time the macroscopic properties of the gas are unchanged. To achieve this the molecular mass m limits to zero in a such way that mN is constant. Furthermore the gas needs to be dilute enough so that multiple particle collisions can be neglected. The Boltzmann-Grad limit can be expressed as

$$Nd^3 \ll \overline{x}^3, \tag{4.5}$$

where d denotes diameter of molecules and $\overline{x}$ is a typical length scale.

As is shown in references [11, 13] to complete and close the hierarchy more assumptions than binary collisions are required. Most important assumption is so-called molecular chaos. This requires that molecules that are about to collide are in a non-correlated state. This could be stated in other words as requirement that the molecules haven't collided with each other in near past. This is an essential a property of randomness and it is very hard to name a system which doesn't fulfill this condition. Once chaos has been established the Boltzmann equation has been shown to asymptotically propagate it.

Final closed equation known as the Boltzmann kinetic equation can be written as (4.6). Term describing the effect of volume forces is omitted on the grounds that it isn't important in the thesis.

$$\partial_t f + \mathbf{u}\cdot\nabla f = Q(f, f') \tag{4.6}$$

On the right side of the equation lies a term called a collision integral Q which expresses change of distribution function due to particle collisions. It is described in further detail in next section.

In the case of extremely rarefied gases the particle collisions can be neglected and the collision integral Q becomes nearly zero. We obtain free transport equation for f (4.7). The operator $\mathbf{v}\cdot\nabla$ is classical transport operator. Solution of hyperbolic free transport equation can be easily obtained analytically. Initial conditions are streamed along characteristic lines.

$$\partial_t f + \mathbf{u}\cdot\nabla f = 0 \tag{4.7}$$

The Boltzmann equation is of integral-differential type. The collision term consists of five dimensional integral over the whole velocity space. That among other things means that it's analytical solution are possible only in very special simple cases.

4.2 Collision Integral

From mathematical point of view the collision integral Q is tensor quadratic operator acting on the velocities $\mathbf{u}$. It is given as

$$Q(f, f') = \int_{R^3} \oint_{|\mathbf{s}|=1} B(\mathbf{u} - \mathbf{u}_*, \mathbf{s})(f' f'_* - f f_*) ds^2 du_*^3. \tag{4.8}$$

We have used standard abbreviations in the field of Boltzmann equation. Velocities $\mathbf{u}$, $\mathbf{u}_*$ are in post-collision state and $\mathbf{u}'$, $\mathbf{u}'_*$ are pre-collision values as is depicted in Figure (4.1). Same notation is valid for indexes of distribution function f before (4.9) and after the collision (4.10).

$$f' = f(\mathbf{x}, \mathbf{u}', t) \qquad f'_* = f(\mathbf{x}, \mathbf{u}'_*, t) \tag{4.9}$$

$$f = f(\mathbf{x}, \mathbf{u}, t) \qquad f_* = f(\mathbf{x}, \mathbf{u}_*, t) \tag{4.10}$$

Collisions are assumed to be binary and elastic. Binary collision proposition is serious difficulty when the density becomes sufficiently large. But in gases it is generally accepted and very accurate approximation. Neglected multi-particle collisions are more frequent than it seems. Interaction potential of molecules can be approximated by a power law. Power law potentials are rapidly decaying but their range is infinite and therefore if the scale is small enough every molecule in the gas is colliding with every other at the same time. Infinite range interaction poses one of the difficulties in analysis of the Boltzmann equation and are usually cut off to ensure finiteness of certain integrals.

During elastic collisions momentum and kinetic energy are the same before and after the collision. Since we are not dealing with mixtures all particles have the same mass and therefore energy and momentum conservation can be stated as

$$\mathbf{u}' + \mathbf{u}'_* = \mathbf{u} + \mathbf{u}_*, \tag{4.11}$$

$$\mathbf{u}'^2 + \mathbf{u}'^2_* = \mathbf{u}^2 + \mathbf{u}_*^2. \tag{4.12}$$

All collisions can be parametrized by assuming a reference system in the plane of collision defined by pre-collisional velocities. Having $\mathbf{s} \in \mathbb{R}^2$, $|\mathbf{s}| = 1$ the pre-collisional velocities can be written as

$$\mathbf{u}' = \frac{\mathbf{u} + \mathbf{u}_*}{2} + \frac{|\mathbf{u} - \mathbf{u}_*|}{2}\mathbf{s}, \tag{4.13}$$

$$\mathbf{u}'_* = \frac{\mathbf{u} + \mathbf{u}_*}{2} - \frac{|\mathbf{u} - \mathbf{u}_*|}{2}\mathbf{s}. \tag{4.14}$$

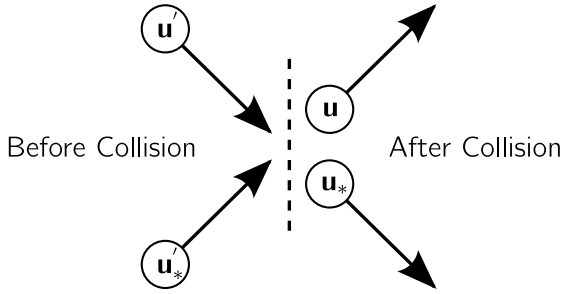

Figure 4.1: Collision Velocities Notation

The difference of products of density distribution functions in the definition of collision integral (4.8) can be split into gain term containing $f^{'}f^{'}_{*}$ and loss term containing ff_{*}. Loss term represents all collisions in which a given particle at velocity $\mathbf{u}$ will encounter another particle and exchange of momentum will lead to a different velocity. The gain term measures the number of particles whose post-collision velocity is $\mathbf{u}$ and have therefore gained this value of velocity due to collisions.

The collision kernel B is always non-negative and depends only on $|\mathbf{u}|$ and $\mathbf{u} \cdot \mathbf{s}$ because elastic collisions are reversible. The collision kernel depends crucially on the microscopic interactions and molecular potentials. Various kinds of collision kernels for different kinds of scattering together with their derivation from microscopic potentials can be found for example in reference [12]. Collision kernel for hard spheres is effectively a cross-section and can be explicitly written as

$$B = d^2|\mathbf{u}|. \tag{4.15}$$

Cercignani in [12] showed that there are only five elementary collision invariants $I(\mathbf{u})$ having the property

$$\int_{\mathbb{R}^3} I(\mathbf{u})Q(f, f^{'})\, du^3 = 0.$$

Namely elementary invariants are a constant, velocity $\mathbf{u}$ and kinetic energy $\mathbf{u}^2$. Since arbitrary constant is also an invariant all the other collision invariants can be constructed as linear combinations of the elementary ones. Cercignani also showed that there exists a family of distribution functions which yields zero collision integral $Q(f^{eq}, f^{eq'}) = 0$. The equilibrium Maxwell distribution function (4.16) is a special case among these functions.

$$f^{eq} = \frac{\rho}{c^3\left(\frac{2\pi}{\gamma}\right)^{3/2}} \exp\left(-\frac{\gamma}{2}\left(\frac{\mathbf{v}-\mathbf{u}}{c}\right)^2\right) \tag{4.16}$$

It is noteworthy to state that f^{eq} depends on spatial coordinate $\mathbf{x}$ and time t only by means of macroscopic variables ρ, $\mathbf{v}$ and c.

4.3 Boundary Conditions

If we are about to describe an experimental setup where gas flows past a solid body or is contained in a region bounded by the domain the Boltzmann kinetic equation must be provided with a boundary conditions. Boundary conditions in a sense represent what is taking place behind them. In the context of Boltzmann kinetic equation boundary conditions model the interaction between gas molecules and the wall. Mechanism of this interaction is responsible for momentum exchange and heat transfer.

In order to write down accurate expressions for the boundary conditions one needs to gain a deep insight to the molecular and in some cases even quantum-mechanical level. The lack of knowledge about the structure of surface layers of solids makes this task quite difficult since molecule impacting upon a surface is adsorbed and various things can occur. It may chemically react and form a bond, dissociate, ionize or even shift the surface molecules.

Boundary conditions are prescribed on a part of the phase space $\partial\Omega^+$ which lies on the boundary of the domain $\partial\Omega$ and have velocities pointing towards the boundary

$$\partial\Omega^{\pm} = \{\mathbf{x} \in \partial\Omega,\ \mathbf{v} \in \mathbb{R}^3,\ \pm\mathbf{v}\cdot\mathbf{dA} > 0\}.$$

dA is unit vector perpendicular to the boundary and pointing outwards.

4.3.1 Reflection

Specular reflection boundary condition is an approximation of gas-surface interaction where molecules bounce back off the surface. It is assumed that the position of the boundary is perfectly known and that the surface is completely smooth. The post-collision angle is the same as pre-collision one as is displayed in Figure 4.2.

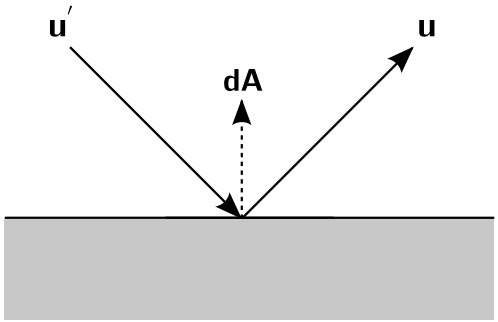

Figure 4.2: Specular Reflection Boundary Condition

Finer details of molecular interaction are not taken into consideration. Mathematical formulation of the boundary condition is

$$\begin{aligned} f(\mathbf{x},\mathbf{u},t) &= f(\mathbf{x},\mathbf{u}',t), \\ \mathbf{u} &= \mathbf{u}' - 2(\mathbf{dA}\otimes\mathbf{dA})\mathbf{u}'. \end{aligned}$$

Specular reflection is an analogy to macroscopic no-slip boundary condition.

4.3.2 Diffusive Scattering

Diffusive scattering is a finer boundary condition taking into account boundary irregularities and scattering on walls

$$f(\mathbf{x}, \mathbf{u}, t) \;=\; \int_{\partial\Omega^+} K(\mathbf{u}, \mathbf{u}') f(\mathbf{x}, \mathbf{u}', t)\; du'^3.$$

K is a scattering kernel responsible for statistical modeling of gas-surface interaction. Choice of scattering kernel K is very complex topic since it must take into account all the phenomena stated above. As demonstration of extent and complexity could serve several chapters devoted to the problematic in monographs [12, 13]. In general post-collision velocities can have arbitrary directions as is displayed in Figure 4.3.

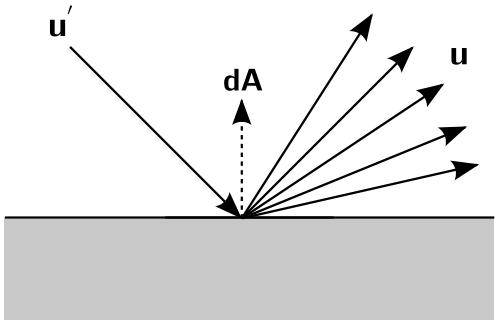

Figure 4.3: Diffusive Scattering Boundary Condition

The scattering diffusion has an analogy in macroscopic boundary condition representing certain amount of slip that is determined by the exact form of the collision kernel.

4.3.3 Maxwell Scattering

Particularly useful example of scattering kernel is Maxwellian reflection

$$f(\mathbf{x}, \mathbf{u}, t) \;= f^{eq}_{\Theta_w} \int_{\partial\Omega^+} f(\mathbf{x}, \mathbf{u}', t)\; du'^3. \tag{4.17}$$

$f^{eq}_{\Theta_w}$ is a Maxwell distribution where local speed of sound is determined by the temperature of the wall Θ_w. This models a process which is a very good approximation to what is taking place on the gas-surface interface if there are no chemical reactions. The molecules are adsorbed and released after it has been heated or cooled to the temperature of the wall. Distribution of velocities corresponds to the equilibrium Maxwell distribution at the temperature of the wall.

4.4 H-Theorem

In the same paper where Ludwig Boltzmann gave a heuristic derivation of equation that now bears his name he also deduced an important consequence from it. Now this result is known as the H-theorem. This theorem explains at fundamental level the irreversibility of natural processes by showing that molecular collisions never decreases entropy density. Entropy density is defined for arbitrary distribution function f satisfying the Boltzmann kinetic equation as

$$h = \int_{R^3} f(\mathbf{x}, \mathbf{u}, t) \log f(\mathbf{x}, \mathbf{u}, t)\ du^3. \tag{4.18}$$

The H-theorem states that

$$\frac{dh}{dt} \leq 0. \tag{4.19}$$

The equal sign is valid only if f is Maxwell distribution function (4.16). There are some issues with integrability of certain the terms when one calculates the full time derivative of entropy density. Due to this sufficiently general proof of the theorem has not been available until recently. The details of the proof are discussed in section 5.6.

It would be tempting in virtue of (4.19) to expect that the solutions of the Boltzmann kinetic equation are more and more resembling the Maxwell distribution as the time progresses. This holds for true for majority of boundary conditions. For example specular reflection or periodic boundary condition. It is also true for unbounded domains. However inappropriate choices of boundary conditions could easily spoil this and establish an equilibrium state different than the one given by the Maxwell distribution function. This is especially true for rarefied gas where gas-surface interaction in some configurations has more influence on establishing equilibrium state than inter-particle collisions.

4.5 Scaling

Dimensionless scaling of the Boltzmann equation happens on two distinct levels. Temperature in Boltzmann equation is represented in a natural way as kinetic energy of molecules and it's value is established only by averaging over the velocity space (4.4). This sets a scale given by the characteristic velocity at microscopic level which we choose as sound speed $\overline{c}$ at reference temperature $\overline{\Theta}$. The microscopic dimensionless velocity is then defined as

$$\widehat{\mathbf{u}} = \frac{\mathbf{u}}{\overline{c}}. \tag{4.20}$$

If we choose reference length $\overline{x}$, time $\overline{t}$, density $\overline{\rho}$, and temperature $\overline{\theta}$ we can start defining dimensionless equivalents of respective macroscopic quantities. If we denote dimensionless equivalent of each macroscopic with hat we arrive at

$$\widehat{\mathbf{x}} = \frac{\mathbf{x}}{\overline{x}}, \quad \widehat{t} = \frac{t}{\overline{t}}, \quad \widehat{\rho} = \frac{\rho}{\overline{\rho}} \tag{4.21}$$

Using dimensionless variables the dimensionless operators evaluate as

$$\widehat{\partial}_t = \overline{t}\,\partial_t, \qquad \widehat{\nabla} = \overline{x}\,\nabla. \tag{4.22}$$

Scaling of distribution function f can be determined from the dimensional analysis and goes as

$$\widehat{f} = \frac{\overline{c}^3}{\overline{\rho}} f. \tag{4.23}$$

Scaling of the collisional operator is a bit more cumbersome. The integrals surrounding the collisional kernel suggests that collision kernel can be interpreted as frequency of collisions happening in a unit mass spread across a unit volume. The characteristic time scale of the collision kernel is determined by the mean time between consecutive collisions $\langle t_\lambda \rangle$. Using the reference speed of sound we can relate $\langle t_\lambda \rangle$ to the mean free path as

$$\overline{c} = \frac{\langle \lambda \rangle}{\langle t_\lambda \rangle}. \tag{4.24}$$

This in turn yields dimensionless collision kernel as

$$\widehat{B} = \frac{\overline{\rho}}{\langle t_\lambda \rangle} B.$$

Finally after substitution of dimensionless variables into the definition of the collision integral (4.8) the dimensionless collisional operator can be written as

$$\widehat{Q} = \frac{\overline{c}^4}{\langle \lambda \rangle \overline{\rho}} Q. \tag{4.25}$$

Having dealt with all the quantities in the Boltzmann kinetic equation it's dimensionless form is

$$Ma\,\widehat{\partial}_t \widehat{f} + \widehat{\mathbf{u}} \cdot \widehat{\nabla}_x \widehat{f} = \frac{1}{Kn}\,\widehat{Q}(\widehat{f}, \widehat{f}^{\,\prime}). \tag{4.26}$$

The mach number Ma was earlier defined in (2.19). However there are some finer details and discrepancies in the definition that need to be discussed. Mach number from the scaling of Boltzmann kinetic equation comes out as

$$Ma = \frac{\overline{x}/\overline{t}}{\overline{c}}. \tag{4.27}$$

Usually the choice of reference quantities $\overline{t}$ and $\overline{x}$ is done in a way that corresponds to the dimensions of the domain and timescale of the gas motion. In some cases the scale of

reference velocity $\overline{v}$ can be small enough so that the scale of $\overline{x}$ and $\overline{t}$ can be seen as some kind of macroscopic flow where the small oscillations of size $\overline{v}$ occurs on top of a much larger flow. Therefore the definition of the Mach number using the reference velocity $\overline{v}$ is invalid and approach though $\overline{x}$ and $\overline{t}$ must be adopted. In the case where the reference space and time scales are in accordance with the velocity scale the problem is no longer important and macroscopic reference velocity can be defined as

$$\overline{v} = \frac{\overline{x}}{\overline{t}}. \tag{4.28}$$

In case of higher Mach number flow microscopic and macroscopic scales start to overlap and it is reasonable to make both velocities comparable and set the reference macroscopic velocity to the sound of speed and introduce dimensionless macroscopic velocity

$$\widehat{\mathbf{v}} = \frac{\mathbf{v}}{\overline{v}} = \frac{\mathbf{v}}{\overline{c}}. \tag{4.29}$$

We have derived that the natural dimensionless scaling parameters are the Mach number and the Knudsen number. Introduction of other commonly used dimensionless scaling parameter the Reynolds number Re is in the context of Boltzmann kinetic equation a bit more cumbersome. Viscous forces are represented only through collision kernel Q and viscosity can be expressed for certain types of collision kernels as an integral as is shown by Chapman and Cowling in [14].

4.6 Hydrodynamic limits

Common way to investigate limiting behavior of Boltzmann kinetic equation is to employ Chapman–Enskog expansion. It consists of expansion in powers of Knudsen number whose value provides a measure of deviation of the Boltzmann distribution from its local equilibrium state. The time scale is expanded on two distinct levels. On the diffusive level and convective level.

Making such limits and expansions mathematically rigorous turned out to be very demanding task and requires introduction of entirely new weak function spaces that suit the particular problem and to large extent suffer from all kinds of child complaints since the field is far from being completely understood. Some details on mathematical advance in investigation of the limits can be found in [10, 11, 12, 35] and references therein.

Chapter 5

Lattice-Boltzmann Method

5.1 BGK Approximation of Collision Integral

The major difficulty when it comes to solving Boltzmann kinetic equation is the collision integral. There have been proposed much simpler descriptions of collision mechanisms to deal with the complexity. Arguably the most popular BGK[1] simplification of the collision integral is to large extent responsible for the success of the method. Original idea goes to classical Brathnagar, Gross and Krook paper [5] where they have applied simplified collision integral (5.1). The idea of the simplification is to remove enormous number two-particle interactions which are unlikely to substantially affect the values of macroscopic quantities by a relaxation towards the equilibrium state.

$$Q_{BGK}(f) = \frac{1}{\tau}\left(f^{eq} - f\right) \tag{5.1}$$

It is easy to see that Q_{BGK} has the same collision invariants as the original collision operator Q provided that the local Maxwell distribution function f^{eq} has the same macroscopic density, velocity and speed of sound.

Rate of relaxation towards Maxwell distribution is governed by relaxation time τ. We can relate the relaxation time to the mean time between molecular collisions $\langle t_\lambda \rangle$ to obtain dimensionless relaxation time

$$\widehat{\tau} = \frac{\tau}{\langle t_\lambda \rangle}.$$

It is not surprising that BGK approximation of the collision integral scales in a very similar fashion to the original collision integral

$$\widehat{Q}_{BGK}(\widehat{f}) = \frac{\overline{c}^4}{\langle \lambda \rangle \overline{\rho}} \frac{1}{\widehat{\tau}} Q_{BGK}(f).$$

The dimensionless Maxwell distribution function which is part of the $\widehat{Q}_{BGK}$ can be written as

[1] BGK are first letters of names of authors who proposed the operator.

$$\widehat{f}^{eq} = \frac{\widehat{\rho}}{\left(\frac{c}{\overline{c}}\right)^3 \left(\frac{2\pi}{\gamma}\right)^{3/2}} \exp\left(-\frac{\gamma}{2}\left(\frac{\overline{c}}{c}(\widehat{\mathbf{v}} - \widehat{\mathbf{u}})\right)^2\right). \tag{5.2}$$

We can write the dimensionless Boltzmann kinetic equation with BGK approximation as

$$Ma\ \widehat{\partial}_t \widehat{f} + \widehat{\mathbf{u}} \cdot \widehat{\nabla} \widehat{f} = \frac{1}{Kn}\ \frac{1}{\widehat{\tau}} \widehat{Q}_{BGK}(\widehat{f}). \tag{5.3}$$

5.2 Discretization of Velocity Space

He in [22] showed that lattice-Boltzmann method can be obtained from the Boltzmann kinetic equation by special discretization of velocity space and use of small Mach number expansion. The starting point of his derivations is Boltzmann kinetic equation with BGK approximation of collision integral (5.3).

In order to deal with unbounded velocity space He adopted approach where only a small number discrete velocities $\widehat{\mathbf{u}}_\alpha$, $\alpha = \{0, ..., L\}$ are chosen and only distribution function evaluated at these velocities are used to determine macroscopic variables. Using notation $\widehat{f}_\alpha(\widehat{\mathbf{x}}, \widehat{t}) = \widehat{f}(\widehat{\mathbf{x}}, \widehat{\mathbf{u}}_\alpha, \widehat{t})$ we can in analogy to (4.1)-(4.4) write

$$\rho_{LB} = \sum_{\alpha=0}^{L} w_\alpha \widehat{f}_\alpha, \tag{5.4}$$

$$\rho_{LB}\mathbf{v}_{LB} = \sum_{\alpha=0}^{L} \widehat{\mathbf{u}}_\alpha\ w_\alpha \widehat{f}_\alpha, \tag{5.5}$$

$$\rho_{LB}\mathbb{P}_{LB} = \sum_{\alpha=0}^{L} \widehat{\mathbf{u}}_\alpha \otimes \widehat{\mathbf{u}}_\alpha\ w_\alpha \widehat{f}_\alpha, \tag{5.6}$$

$$\rho_{LB} e_{LB} = \sum_{\alpha=0}^{L} \widehat{\mathbf{u}}_\alpha^2\ w_\alpha \widehat{f}_\alpha. \tag{5.7}$$

Indexes $_{LB}$[2] signify that the respective quantity is a discrete lattice-Boltzmann counterpart of the original physical value. To obtain exact values of weights w_α Shan in [36] used Gauß-Hermite quadrature of 3^{rd} order and pointed out that in order to recover isothermal Navier-Stokes equations integrals of powers of microscopic velocity up to $\int_{\mathbb{R}^3} \mathbf{u}^3 f^{eq}\ du^3$ must be evaluated exactly by the quadrature. To recover non-isothermal hydrodynamics moments of up to 4^{th} order of $\mathbf{u}$ must be exact. The values of the w_α and orientation of discretization velocities $\widehat{\mathbf{u}}_\alpha$ for widely used isothermal D2Q9 velocity model are displayed in Figure 5.1. Weights for many other velocity discretizations can be found in paper [21].

It is common in the field to adopt DNQL notation for categorization of velocity models. Number N stands for spatial dimensions and L stands for number of discrete velocities used to

[2] LB is acronym of lattice-Boltzmann.

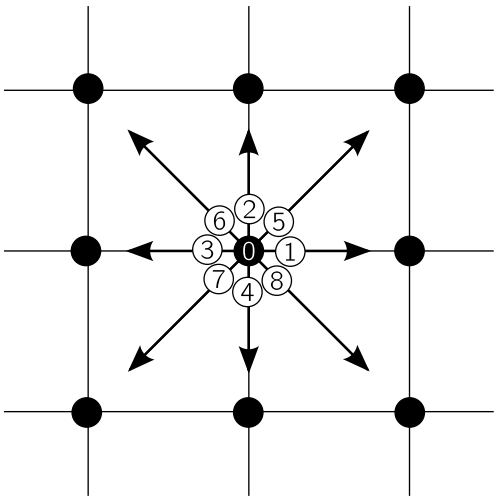

w_α	α
4/9	0
1/9	1 2 3 4
1/36	5 6 7 8

Figure 5.1: Isothermal D2Q9 Velocities and Weights

evaluate the quadratures (5.4)-(5.7) at each point of space. Straightforward extension of the D2Q9 model into 3D is D3Q27 which is essentially three D2Q9 models from Figure 5.1 layered on top of each other to achieve 3D structure of the discretized velocity vectors $\widehat{\mathbf{u}}_\alpha$.

We introduce effective distribution function $F_\alpha = w_\alpha \widehat{f}_\alpha$ and since weights and discrete velocities are constants we can write in virtue of (5.3) the following system of equations which holds at each point in space

$$Ma\, \widehat{\partial}_t F_\alpha + \widehat{\mathbf{u}}_\alpha \cdot \widehat{\nabla} F_\alpha = \frac{1}{Kn}\, \frac{1}{\widehat{\tau}} \left(F_\alpha^{eq} - F_\alpha\right),\ \alpha = \{0, ..., L\}. \tag{5.8}$$

If we approximate the time derivative by 1^{st} order finite difference and the convective term by a 1^{st} order upwind finite difference we arrive at discrete version of equation (5.8)

$$\begin{aligned} F_\alpha(\widehat{\mathbf{x}}, t+\delta_t) - F_\alpha(\widehat{\mathbf{x}}, t) + \underbrace{\frac{|\widehat{\mathbf{u}}_\alpha|}{Ma}\frac{\delta_t}{|\delta_{\mathbf{x}\alpha}|}}_{1} \left(F_\alpha(\widehat{\mathbf{x}}, t) - F_\alpha(\widehat{\mathbf{x}} - \delta_{\mathbf{x}\alpha}, t)\right) = \\ = \underbrace{\frac{\delta_t}{Kn\ Ma}}_{1}\, \frac{1}{\widehat{\tau}} \left(F_\alpha^{eq}(\widehat{\mathbf{x}} - \delta_{\mathbf{x}\alpha}, t) - F_\alpha(\widehat{\mathbf{x}} - \delta_{\mathbf{x}\alpha}, t)\right),\ \alpha = \{0, ..., L\}. \end{aligned} \tag{5.9}$$

The reason why collision terms are discretized by downwind finite difference is not clear at the first sight. Chen in [16] showed that although it is not obvious the delicate Lagrangian nature of the discretization is capable of achieving 2^{nd} order accuracy both in space and time.

By choosing multiplicative factors that came out of discretization to be 1 we recover the Lattice Boltzmann equation (5.10).

$$F_\alpha(\widehat{\mathbf{x}} + \delta_{\mathbf{x}\alpha}, t+\delta_t) = F_\alpha(\widehat{\mathbf{x}}, t) + \frac{1}{\widehat{\tau}} \left(F_\alpha^{eq}(\widehat{\mathbf{x}}, t) - F_\alpha(\widehat{\mathbf{x}}, t)\right),\ \alpha = \{0, ..., L\}. \tag{5.10}$$

5.3 Lattice

To finish the discretization and complete the lattice-Boltzmann model algorithm we need to discuss how are the space and time discretization tied together. The discretization forms so-called lattice as can be seen in Figure 5.1. In the field of lattice-Boltzmann equation term lattice is utilized to refer to the structure of space discretization. It can be considered as an analogy to mesh used in traditional CFD.

Lattice is a periodic structure consisting of nodes denoted by black circles where the distribution function is evaluated. Distance of the neighbor nodes is a natural lattice length unit. One iteration over all the nodes advances the time by one lattice time step which is in a similar way natural unit of time on the lattice. The adjacent nodes are inter-connected by discretization velocities in such a way that that spatial step is related to the time step by Lagrangian relation

$$\delta_{\mathbf{x}\alpha} = \widehat{\mathbf{u}}_\alpha \delta_t, \ \alpha = \{0, ..., L\}.$$

We have in the last step of derivation of the velocity space assumed that

$$Ma = c_{LB} \frac{|\delta_{\mathbf{x}\alpha}|}{\delta_t}. \tag{5.11}$$

We have denoted the size of $\widehat{\mathbf{u}}_\alpha$ as c_{LB} which is lattice speed of sound. For particular velocity discretization it is a fixed constant. In fact no information on the lattice can propagate faster than c_{LB}. For D2Q9 velocity model the lattice speed of sound attains value of $\frac{1}{\sqrt{3}}$. Impossibility to change the speed of sound is one of the main drawbacks of the lattice-Boltzmann method.

The discretization has another minor drawback which is an assumption that ties together Mach and Knudsen number

$$Ma = \frac{1}{\delta_t} Kn. \tag{5.12}$$

However this assumption is not so severe in incompressible the applications since value of Ma is considered negligible.

While in traditional CFD the local refinement of mesh is mandatory for efficient and accurate solution. In case of the lattice this brings difficulties and the topic is a subject of active research.

Explicit nature of lattice-Boltzmann discretization suggest that when the lattice is refined the time step must be decreased correspondingly to keep the speed of sound constant at all levels. Besides the time step complication which is manageable deeper analysis [19] shows that values of distribution function cannot be transferred or interpolated directly in places where the coarser part of lattice meets the finer one. The macroscopic fluid dynamic variables like viscosity or heat conductivity must be kept smooth on the interface. These two effects spoil significant amount the effort invested into lattice refinement techniques but performance boost is still achievable.

5.4 Discretization of BGK Approximation

For the isothermal D2Q9 velocity the ratios of $c/\bar{c}$ are 1 and dimensionless Maxwell distribution (5.2) attains much simpler form. In order to derive the velocity model weights Shan replaced the dimensionless Maxwell distribution by Taylor series expansion in dimensionless macroscopic velocity $\widehat{\mathbf{v}}$ up to 2^{nd} order and obtained effective discretized equilibrium distribution function

$$F_{\alpha}^{eq} = \frac{w_{\alpha}\widehat{\rho}}{\left(\frac{c}{\bar{c}}\right)^{3}\left(\frac{2\pi}{\gamma}\right)^{3/2}} \exp\left(-\frac{\gamma}{2}\widehat{\mathbf{u}}_{\alpha}^{2}\right)\left(1+\gamma\widehat{\mathbf{u}}_{\alpha}\cdot\widehat{\mathbf{v}}+\frac{1}{2}\left(\gamma\widehat{\mathbf{u}}_{\alpha}\cdot\widehat{\mathbf{v}}\right)^{2}-\frac{\gamma}{2}\widehat{\mathbf{v}}^{2}\right),\ \alpha=\{0,...,L\} \tag{5.13}$$

For other velocity models than D2Q9 the Maxwell distribution function Taylor series expansion is truncated at higher order to obtain more accurate evaluation of moments of distribution function and recover compressible, thermal or other models. Form of F_{α}^{eq} has to ensure that the macroscopic fluid equation obtained from (5.10) by the Chapman-Enskog expansion agrees with the appropriate limiting macroscopic equations. Exact form of Taylor series expansion depends on the structure of the lattice and is not uniquely determined. This leaves space for improvements in stability or introduction of additional physical phenomena which occur further off the equilibrium state.

Truncated expansion is reasonably accurate as long as the dimensionless velocity $\widehat{\mathbf{v}}$ is small. Considered the definition of the dimensionless macroscopic velocity (4.29) the expansion effectively restricts the local Mach number to small values. Such restriction is only valid for incompressible or very slightly compressible flows. Compressibility in this context is understood differently. Limiting behavior of the truncated series up to 2^{nd} order by no means recovers compressible Navier-Stokes equations.

Instead of solving additional Poisson equation for pressure lattice-Boltzmann method exhibits quasi-compressible behavior in a sense that if the relative fluctuations of density are small then incompressible Navier-Stokes behavior is recovered accurately as the effect of compressibility can be made of the same order as discretization error.

Obviously Taylor series expansion of the equilibrium distribution function is the bottleneck in our discretization. It restricts magnitude of Mach numbers that the method is capable of simulating. As will be discussed later it seems that there are no results that have successfully overcome this difficulty so far.

5.5 Lattice-Boltzmann Method

Lattice-Boltzmann equation (5.10) derived in the previous chapter has many very nice properties. From the numerical point of view the scheme of lattice-Boltzmann equation is explicit. There is no need to solve additional system of equations to advance the time step. Boltzmann kinetic equation can therefore be understood at a more elementary level by using methods original to the lattice-gas automaton.

The calculations are effectively split into two parts as is indicated in (5.14). In the first part the distribution function is streamed alongside velocities $\widehat{\mathbf{u}}_\alpha$ to the nearest neighbor node and after the streaming the relaxation takes place. Relaxation can be interpreted as a simplification of the collision processes in gases that lead towards towards establishing equilibrium.

$$\underbrace{F_\alpha(\widehat{\mathbf{x}} + \delta_{\mathbf{x}\alpha}, t + \delta t) = F_\alpha(\widehat{\mathbf{x}}, t)}_{\textit{Streaming}} \quad \underbrace{-\frac{1}{\widehat{\tau}}\left(F_\alpha^{eq}(\widehat{\mathbf{x}}, t) - F_\alpha(\widehat{\mathbf{x}}, t)\right)}_{\textit{Relaxation}}, \ \alpha = \{0, ..., L\} \tag{5.14}$$

Relaxation and streaming processes in case of the D2Q9 velocity model is displayed on Figure 5.2.

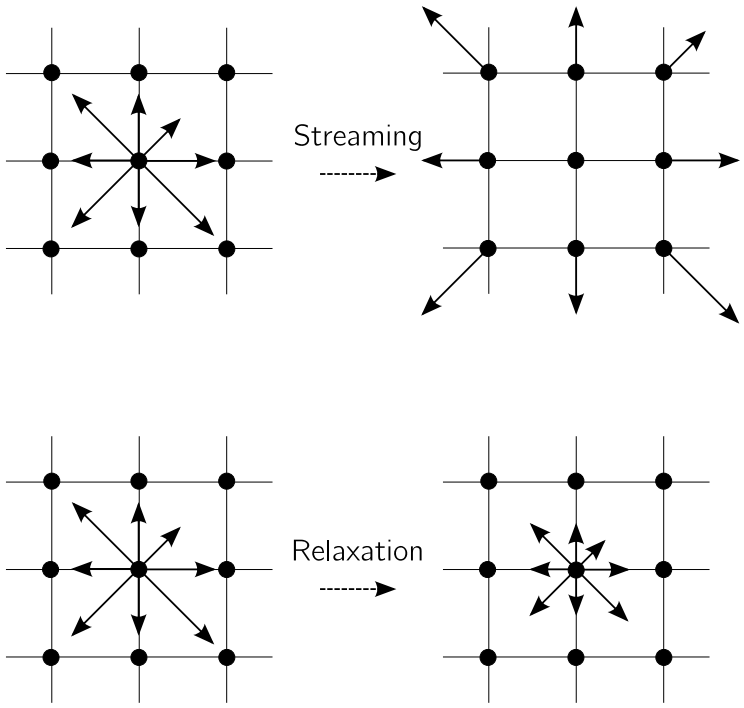

Figure 5.2: D2Q9 Streaming and Relaxation

Convective term represented by streaming operation is non-local since it affects also adjacent nodes but more importantly is linear. Non-linearity is concentrated only in the relaxation step that happens locally. This is major advantage compared to the traditional CFD. The convective term $\nabla \cdot (\mathbf{v} \otimes \mathbf{v})$ is nonlinear and non local at the same time. The fluid momentum is transported along streamlines. In case of case porous media flows the streamlines can have very high derivatives. Rapidly varying velocity negatively affects numerical stability of traditional CFD methods. This effect is completely avoided by the lattice-Boltzmann method.

Another property to notice is that localization of the respective steps in lattice-Boltzmann method makes up for almost ideal scaling in parallel computing since very little communications is required when the domain is split between several computers.

5.6 Hydrodynamic limits

In order to determine limiting behavior of lattice models Chapman-Enskog expansion is used. Typically distribution function is expanded formally into a series around local equilibrium distribution function and time derivatives are considered on two separate timescales. This approach is slightly misleading and the same results can be obtained in more transparent fashion.

In our derivation we consider hydrodynamic limit where Knudsen number is sufficiently small. Knudsen number can be in viewed as a parameter which measures departure off the local equilibrium state. We expand effective distribution function F_α around equilibrium state F_α^{eq} into series of Kn and truncate the series at first non-equilibrium contribution F_α^{neq}

$$F_\alpha = F_\alpha^{eq} + Kn\, F_\alpha^{neq},\ \alpha = \{0, ..., L\}.$$

Since we want our approximation to conserve mass and momentum from (5.4) and (5.5) one can easily deduce following restrictions on F_α^{neq}

$$\sum_{\alpha=0}^{L} F_\alpha^{neq} = 0 \quad , \quad \sum_{\alpha=0}^{L} \widehat{\mathbf{u}}_\alpha F_\alpha^{neq} = \mathbf{0}.$$

Insertion of Knudsen number expansion series into continuous lattice-Boltzmann equation (5.8) yields

$$Ma\ \partial_t \left(F_\alpha^{eq} + Kn\, F_\alpha^{neq}\right) + \widehat{\mathbf{u}}_\alpha \cdot \nabla \left(F_\alpha^{eq} + Kn\, F_\alpha^{neq}\right) = -\frac{F_\alpha^{neq}}{\widehat{\tau}},\ \alpha = \{0, ..., L\}.$$

We have effectively recurrent relation for F_α^{neq} where it is expressed as certain mixtures of it's own spatial and time derivatives. By reinserting the recurrent relation into itself and comparing terms of order Kn^0

$$Ma\ \partial_t F_\alpha^{eq} + \widehat{\mathbf{u}}_\alpha \cdot \nabla F_\alpha^{eq} = -\frac{F_\alpha^{neq}}{\widehat{\tau}},\ \alpha = \{0, ..., L\}.$$

Terms of order Kn^1 can be after non-negligible amount of algebra expressed as

$$Ma\ \partial_t F_\alpha^{neq} + (2\widehat{\tau} - 1)\widehat{\mathbf{u}}_\alpha \cdot \nabla \left(\partial_t F_\alpha^{neq} + \widehat{\mathbf{u}}_\alpha \cdot \nabla F_\alpha^{neq}\right) = 0,\ \alpha = \{0, ..., L\}.$$

Finally after summing over all discretization velocities we can write the conservation equations for lattice mass and momentum as

$$\partial_t \rho_{LB} + \rho_{LB} \nabla \cdot \mathbf{v}_{LB} = 0,$$

$$\rho_{LB} \partial_t \mathbf{v}_{LB} + \nabla \cdot \mathbb{P}_{LB} = 0.$$

The lattice pressure tensor came out as

$$\mathbb{P}_{LB} = \sum_{\alpha=0}^{L} \widehat{\mathbf{u}}_\alpha \otimes \widehat{\mathbf{u}}_\alpha \ \left(F_\alpha^{eq} + (2\widehat{\tau} - 1)F_\alpha^{neq}\right).$$

From the structure of the pressure tensor one can see that viscosity is generally non-equilibrium effect in the Boltzmann kinetic equation. Hydrodynamic limit of zero order expansion which is effectively equilibrium distribution function can be easily identified as Euler equations.

After substitution of equilibrium distribution function (5.13) the pressure tensor can be written as

$$\mathbb{P}_{LB} = \underbrace{\rho_{LB} c_{LB}^2}_{p_{LB}} \mathbb{I} + \rho_{LB} \sum_{\alpha=0}^{L} \widehat{\mathbf{u}}_\alpha \otimes \widehat{\mathbf{u}}_\alpha + \underbrace{(2\widehat{\tau} - 1)}_{\nu_{LB}} \sum_{\alpha=0}^{L} \widehat{\mathbf{u}}_\alpha \otimes \widehat{\mathbf{u}}_\alpha F_\alpha^{neq}.$$

In order to obtain incompressible Navier-Stokes equations we identify previously unspecified dimensionless relaxation time $\widehat{\tau}$ as a way to regulate viscosity

$$\nu_{LB} = (2\widehat{\tau} - 1)c_{LB}^2. \tag{5.15}$$

Another result is that we have derived relation that can be called lattice equation of state. Since c_{LB} is fixed constant when expressed in lattice units we can easily convert between pressure and density when a need arises

$$p_{LB} = c_{LB}^2 \rho_{LB}. \tag{5.16}$$

5.7 Initial and Boundary Conditions

The simplest way to initialize the computation based on lattice-Boltzmann method is to specify an initial macroscopic variables and set all particle distributions to equilibrium based on these using (5.13). But according to Skordos it is slightly inaccurate. In [41] he presented new approach how invert relations (5.4)-(5.7) to calculate the lattice-Boltzmann distribution functions at a boundary node from the fluid variables that are specified at this node. These two approaches are most widely used in lattice-Boltzmann method.

Fluid in simulation is enclosed in a bounded domain and confined by a surrounding boundary. Generally the problem of formulating boundary conditions for lattice-Boltzmann method consist in finding dependence of unknown outgoing particle populations on known incoming populations. Outgoing populations fulfill condition $\widehat{\mathbf{u}}_\alpha \cdot \mathbf{dA} > 0$ where $\mathbf{dA}$ is outer normal to the boundary. Incoming populations are defined by the opposite sign of the inequality. Boundary conditions for lattice-Boltzmann method have in general very weak connection to their continuous counterparts formulated for Boltzmann kinetic equation.

The problem of formulating boundary condition is demonstrated in the case of D2Q9 velocity model in Figure 5.3. Grayed numbers represent outgoing distribution functions which needs to be determined while white number are incoming distribution functions.

Only requirement that needs to be met in order to recover hydrodynamic limits of lattice-Boltzmann equation is conservation of macroscopic variables. This leads to a incomplete system of equations that lacks unique solution. Requirement to complete the system of equations opens up opportunities to add new physical phenomena into the boundary conditions. But this is double-edged sword since caution is required to prevent mathematical ill-posedness and jeopardy of second order of accuracy achieved in discretization.

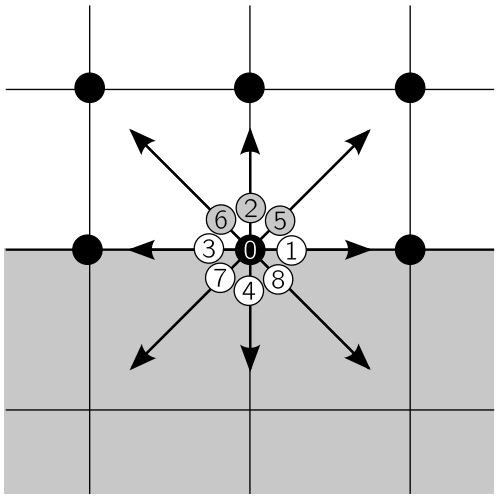

Figure 5.3: D2Q9 Velocities on Boundary

5.7.1 Bounce Back Boundary Condition for Velocity

One of the most basic boundary conditions for lattice-Boltzmann method is a hard wall which reflects particles back and effectively represents a no-slip condition. There exists two variations of this condition the full-way or on-grid bounce-back and the half-way or mid-grid bounce back method.

In both variants boundary conditions are represented by certain nodes on the lattice marked as walls. Such nodes are not part of the fluid and the particle distributions are not relaxed towards equilibrium and are not governed by the lattice-Boltzmann equation.

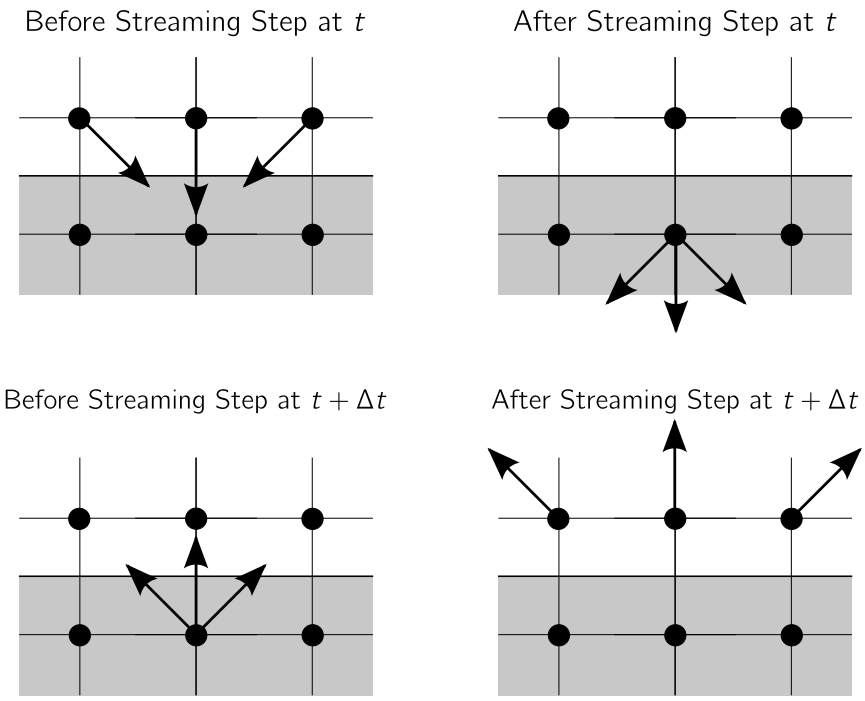

Figure 5.4: Full-way Bounce Back Boundary Condition

The full-way is the simpler of the two methods. In the collision step of each iteration when the fluid nodes are relaxed, all distribution functions residing on bounce back nodes are reversed. That way the particles are sent back in the direction they originally arrived in but one iteration delayed. Collision step is modified for the full-way bounce back nodes but the streaming step is kept the same. Full-way boundary condition is displayed on Figure 5.4.

In the half-way variant, distribution functions that are about to stream into a wall node are reflected instead of streamed, as is depicted in Figure 5.5. In this case the streaming step is modified while the collision step remains the same.

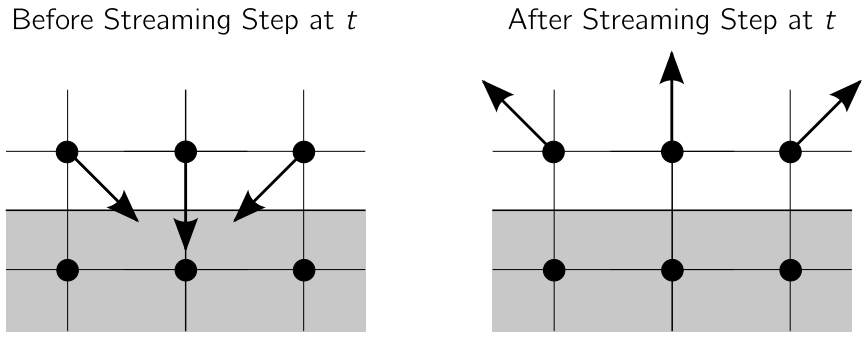

Figure 5.5: Half-way Bounce Back Boundary Condition

In both bounce back conditions the effective position of the wall is actually between the wall nodes and fluid nodes adjacent to it. Half-way bounce back is a more difficult to implement

than the full-way method, but as was shown by Chen in [37] the half-way variant gives second order accuracy which is in agreement with the order of accuracy of lattice-Boltzmann equation. The full-way is only first order accurate. Main difficulties in implementation of the half-way boundary condition are corners. The full-way bounce back node doesn't require any supplemental information about being a corner or regular wall node. The half-way variant demand this information. In 2D there is only inner and outer corner so that doesn't present a limitation. But for example in porous media flow in complex domains where especially in three dimensions situation becomes a bit more cumbersome but still somewhat manageable.

5.7.2 Zou's Boundary Condition for Pressure

Incompressible lattice-Boltzmann method schemes don't deal easily with pressure boundary conditions. The reason behind it is that density and pressure are tied up together by lattice equation of state (5.16). Any pressure change is inevitably accompanied by pressure change which breaks the incompressibility condition in the first place. Conventional CFD typically sweeps the problem under the carpet by allowing arbitrary high speed of sound. That way significant pressure drops can be sustained with negligibly small variation of density and solenoidality of the velocity field is maintained.

In lattice-Boltzmann method steady states are always affected by a compressibility error. It can be estimated by slight modification of continuity equation (3.1). Expanding the divergence term yields

$$\partial_t \rho + \nabla \rho \cdot \mathbf{v} + \rho \nabla \cdot \mathbf{v} = 0. \tag{5.17}$$

If we assume the system in a steady state the time derivative disappear and the resulting equation can be written as

$$\nabla \log \rho \cdot \mathbf{v} + \nabla \cdot \mathbf{v} = 0. \tag{5.18}$$

It's obvious that first term expresses deviations from solenoidal velocity field. In other words compressibility error. The error is of order Ma^2 thus negligible in most applications.

The standard way to impose pressure differences in open flows consists of replacing real pressure gradient with a corresponding volume force producing exactly the same momentum input to the flow as would the pressure gradient. Such procedure breaks down if detailed information about space distribution of the pressure field is required since it's unable to provide this data.

Quasi compressible pressure boundary condition proposed by Zou and He in [49] uses relatively simple strategy as opposed to strictly incompressible approaches in used by Noble in [30]. Drawback of their approach is that in order to calculate missing distribution functions they assumed the tangential components of velocity to be zero. So far there seems to be no way to resolve this problem and not introduce other issues in available literature.

5.7.3 Inamuro's Boundary Condition for Velocity

Inamuro's boundary conditions can be used to represent slip velocity boundary condition. In our case we use only zero slip velocity boundary condition but the original reference [23] deals with arbitrary slip value. Inamuro's boundary condition draws unknown distribution functions from a local equilibrium distribution function with the same normal and different tangential sped at the wall. It can be considered a discrete counterpart continuous of Maxwell scattering (4.17).

Tangential speed is adjusted for so called counter-slip speed to achieve mass flux conservation on the wall. Unknown distribution function at the wall are assumed to be an equilibrium function with a counter-slip velocity which is determined so that fluid velocity at the wall in accordance with the wall velocity and also temperature.

Inamuro and his colleagues tested their boundary condition in two dimensional Poiseuille flow and showed that no-slip condition is accurately reproduced for larger range of relaxation times $\frac{1}{2} < \widehat{\tau} < 20$ whereas standard bounce back condition yields significant error already beyond $\widehat{\tau} < 2$. This is in line with physical expectations since $\widehat{\tau}$ increases with mean free path. Important advantage of this boundary condition over many others is easy transfer into 3D.

Naive attempt to design a zero density gradient might just be to copy the incoming particle population at the outlet. Such a procedure would receive zero gradient but unfortunately doesn't work. The copying produces spurious chain of backward waves of density fluctuations going towards inlet. The fluctuation caused by waves can easily destabilize whole computation. However there are some special cases where it might work. It would be when the density gradients itself would come out small enough for example at the end of a very long channel.

5.7.4 Other Boundary Conditions

The list of boundary conditions presented in the current section is far from complete. An important property of each boundary condition is locality. It is clear from aforementioned descriptions of different boundary conditions that evaluation of missing particle populations involve only direct neighbors of the particular node. Generally non-local boundary condition are better avoided since they spoil linear parallelization scaling which is the most potent advantage of lattice-Boltzmann algorithm over traditional CFD methods.

It's noteworthy that there exist whole family of special boundary conditions designed for multiphase and multi-component flows dealing with various circumstances appearing in the simulations of vapor-liquid mixtures.

We also haven't mentioned so-called complex boundary conditions. We were fortunate enough that the domain setup required for rarefied flow doesn't include any misaligned or curved boundaries. Complex boundary conditions are not easy to implement but results are worth the trouble since they increase order of accuracy as was shown by Renwei [33].

Another thing we haven't noted are periodic boundary conditions. Periodic boundary conditions mainly used in acoustics and unbounded domain simulation. Periodicity is surprisingly easy to implement in lattice-Boltzmann method. The distribution functions will simply reappear on the other side of the domain and continue streaming in the same direction. That way the

system becomes closed by the edges of the domain.

5.8 Lattice Boltzmann Units

5.8.1 Conversions of Units

Conversion of units in physics is generally considered annoying but a simple task. In the case of lattice-Boltzmann method it is not so straightforward one can get completely confused. There are many arguments and notations from different fields that are overlapping. In this section we use a notation concept for conversion between physical and lattice variables introduced earlier. For each physical variable there's a counterpart in lattice units denoted with lower indexes $_{LB}$. Conversion factor between physical and lattice units is denoted as δ with an index representing which quantity is converted.

Natural choice of length unit in a lattice is a distance between adjacent nodes. Values of length on the lattice x_{LB} are integer multiples of the distances between neighboring nodes. Physical and lattice lengths are converted as in

$$\mathbf{x} = \delta_x \, \mathbf{x}_{LB}. \tag{5.19}$$

Length conversion factor δ_x can be found if we divide physical dimension of the system by the number of lattice nodes that represents the distance on the lattice. For example if D is the width of channel in Poiseuille flow and the number of lattice nodes which represent the width is N_D the length conversion factor is $\delta_x = D/N_D$. Conversion factor δ_x can be understood as size of one lattice inter-space in meters.

Similar approach can be used in time conversion. We discretize characteristic time scale T by N_T iteration steps. Therefore time conversion factor is defined as $\delta_t = T/N_T$ and the conversion of lattice iteration steps into physical time goes as

$$t = \delta_t \, t_{LB}. \tag{5.20}$$

Having converted the time and distance one readily gets conversion relation for velocities

$$\mathbf{v} = \frac{\delta_x}{\delta_t} \, \mathbf{v}_{LB}. \tag{5.21}$$

In analogy to previous conversions of length and time we can easily introduce a conversion equation for mass. However following approach introducing densities before mass is more beneficial due to the fact that density is one of the main macroscopic quantities of interest in typical lattice-Boltzmann problem.

Lattice density ρ_{LB} is defined in (5.4). We want the lattice density to be corresponding to the physical density of the gas. In incompressible flow absolute value of lattice density is to a large extent arbitrary and unimportant. Only gradients of the density have significant effects on the fluid dynamics. From the numerical point of view absolute value of lattice density is chosen at the beginning of the computation as an initial value $\overline{\rho_{LB}}$. We generally want the

variations of lattice density to be small compared to it's absolute value. Reason behind it is that magnitude of $\log \rho$ in (5.18) would yield significant deviations from incompressibility if the density is close to zero. In compressible flow one doesn't have this luxury of arbitrary density to improve numerical stability.

Generally accepted scheme is to set the initial lattice density $\overline{\rho}$ very close to 1. If $\overline{\rho}$ denotes the physical value of density corresponding to the initial lattice density $\overline{\rho_{LB}}$ we can introduce density conversion factor δ_ρ in (5.22).

$$\overline{\rho} = \delta_\rho \, \overline{\rho_{LB}} \tag{5.22}$$

Equation (5.22) has a slightly different character than aforementioned conversion equations. It serves as definition of density conversion factor δ_ρ. Actual densities resulting from lattice-Boltzmann method are converted as in (5.23) and the conversion factor value is determined from (5.22).

$$\rho = \delta_\rho \, \rho_{LB} \tag{5.23}$$

In a typical incompressible lattice-Boltzmann simulation [27, 45] conversion factor of density δ_ρ is considered to be 1 and relations (5.22) and (5.23) are not needed at all. Since we are dealing with compressible case and we wish compare them with experiments we are forced to employ it.

Density conversion factor can be expressed as a function of in some sense more fundamental conversion factors for mass δ_m and length δ_x

$$\delta_\rho = \frac{\delta_m}{\delta_x^3}. \tag{5.24}$$

Analogously to the aforementioned conversion one can write relation between mass in lattice and physical units as

$$m = \delta_m \, m_{LB}. \tag{5.25}$$

The last important quantity appearing in our problem that is left to convert is pressure. We need to find the lattice density ρ_{LB} as a function of physical pressure p because values of boundary conditions are given in lattice densities rather than pressures. Lattice pressure and density are constrained by the lattice equation of state (5.16).

Considering the units of pressure one can readily obtain the relation for conversion

$$p = \frac{\delta_m}{\delta_x \delta_t^2} \, p_{LB}. \tag{5.26}$$

Substituting the mass conversion factor δ_m as defined by (5.24) and lattice equation of state we can simplify pressure conversion to

$$p = \frac{\delta_\rho \delta_x^2}{\delta_t^2} \, c_{LB}^2 \rho_{LB}. \tag{5.27}$$

5.8.2 Choice of space and time step

The largest difficulty is that in lattice-Boltzmann method the value of the Mach number is coupled with the choice of the discrete time and space step by (5.11). The speed of sound is a lattice constant independent of time and length conversion factor. This means that if the values of space and time steps are not chosen appropriately the physical $\overline{c}$ and lattice speed of sound c_{LB} don't attain the same value

$$\overline{c} = \frac{\delta_x}{\delta_t} c_{LB}. \tag{5.28}$$

Discrepancy between real and lattice-Boltzmann speed of sound is not an issue in applications that intend to recover the incompressible Navier-Stokes equation in the limit because the sound speed is typically not the point of interest. More important is the correct value of viscosity which in turn yields the same value of Reynolds number in the physical and computational system. From the conversion formalism introduced in the previous chapter it easily follows that conversion of viscosity into physical units goes as

$$\nu = \frac{\delta_x^2}{\delta_t} c_{LB}^2 (2\widehat{\tau} - 1).$$

We have used the relation for lattice viscosity (5.16). Choice typically observed in the literature is to change scaling parameters in such way that Reynolds number which is proportional to the inverse of the viscosity remains constant.

Scaling in acoustic applications go exactly the other way. Speed of sound is crucial for validity of the results therefore the scaling is based on (5.28). This essentially means that proper wave dispersion can't be predicted using the lattice-Boltzmann method as is shown by Viggen in [45].

Scaling used in the thesis comes from high Knudsen number flows in MEMS devices and is chosen to be

$$Kn = \delta_x \widehat{\tau}. \tag{5.29}$$

It is interesting to note that many other variations are actively used. Basic thing on what the authors of available papers disagree is the multiplicative constant before Kn. Nie in [29] determines the constant by fitting numerical results on experimental data. The fitted value is very closed to value used by Zhang in [48] or Kim in [25]. Succi [43, 44] and some other authors offset the value of relaxation time $\widehat{\tau}$ by $1/2$ but this is only convention since values of $\widehat{\tau}$ below $1/2$ lead to numerical instabilities due to negative viscosity.

5.9 Limitations

5.9.1 Stability

The Chapman-Enskog expansion verifies how the model will behave on in hydrodynamic long-wavelength limit however it guarantees very little about the model's behavior at shorter

scales. Stability question of lattice-Boltzmann method is still an open one.

There's restriction on relaxation time $\widehat{\tau} > 1/2$ given by the positivity of viscosity. Another problem discussed earlier is that lattice velocities needs to be kept sufficiently small in order for the computation to be stable. That is because model doesn't support supersonic flows. As the structure of discretized equilibrium distribution function (5.13) suggests if lattice velocities reach values comparable with the speed of sound the calculation yields infinite results as a consequence of negative densities.

The discretized equilibrium distribution function is not always positive as it's continuous counterpart. This effect is technically prevented in entropic lattice-Boltzmann methods proposed recently by Karlin in [18] that fulfill the discrete version of the H-theorem. Lattice densities needs to be offset from zero in order to avoid locally negative distribution functions and achieve small variations. Chen and Sterling provided survey of the problem in [16]. Their results are consistent with the overall framework of the lattice-Boltzmann method.

From von Neumann stability analysis they concluded limit on the relaxation time $\widehat{\tau}$ is consistent with positivity of the viscosity. They also derived upper limit on the velocity than can be achieved on the lattice which fits into the scheme of low Mach number expansion employed to derive the discretization of velocity space. Although their results apply in the simple geometry of Poiseuille channel. More general results are not available as far as author is aware.

5.9.2 High Mach Number

Dimensionless equilibrium distribution functions (5.2) in isothermal models has the constant reference sound of speed $\overline{c}$ appearing in the denominators as opposed to thermal models where the speed of sound c can't be considered constant. Therefore non-dimensional velocity $\widehat{\mathbf{v}}$ based on a dynamic speed of sound produces additional terms in time and space derivatives. This presents a problem for Gauß-Hermite expansion. To overcome such difficulty different approach was proposed by Shan in [38]. The continuous Boltzmann kinetic equation with BGK collision operator is projected on special basis consisting of Gauß-Hermite polynomials and truncated at appropriate order. This problem has also implications at higher Mach numbers.

The range of *Ma* that occurs in the multiorifice experiment is approximately 0.3-0.5 as can be seen in figure (2.19). Locally one can expect the *Ma* to be even higher. The Mach number is determined from the average velocity of the flow and reference temperature. If gas flow would be fully developed and no-slip boundary condition would hold on the walls of channels the maximal velocity would be $3/2$ of the average as can be easily calculated from analytic solution Navier-Stokes equation in configuration of Poiseuille flow. Despite flow through multiorifice is anything but fully developed such simplified approximation allows to estimate that local Mach numbers can even reach values around 0.8.

There are many quite successful results in the open literature that use compressible lattice-Boltzmann method limiting in Euler equations. However the list is narrowed down significantly when one states the requirement of proper compressible viscous flow treatment. The reason behind it needs to be looked for in intrinsic nature of lattice-Boltzmann discretization that

ties together the speed of sound and viscosity which seems to be extremely hard to overcome without spoiling other benefits of the discretization.

Sharipov used DSMC method mentioned in early chapters to calculate flow rates of thin orifice in [39]. From the results part it can be clearly seen that the temperature along the axis of the orifice changes significantly. Rescaling his results to our case yields downstream temperature of 60 K. Drop in temperature is caused by nearly adiabatic expansion of gas into vacuum. Process can be considered adiabatic due to fact that in rarefied gas viscous heating and heat exchange can be neglected under the circumstances. Quick estimate shows that drop in temperature means that the sound speed decreases locally in the downstream area of the orifice to about a half of the upstream value. This argumentation can be numerically verified in Sharipov's other paper on outflow of long tubes into vacuum [40] where it can be seen that in similar computational configuration locally the Mach number reaches values up to 2.0.

5.10 Proposed Modifications

From the earlier discussion it turned out that in order to describe the situation that arise in the multiorifice experiment isothermal lattice-Boltzmann method capable of reaching Ma around 1.0 would be desirable. Although at the same time the method must remain stable at large relaxation times $\widehat{\tau}$ as is the case in rarefied flows and must be able to recover proper value of viscosity.

Chen and his colleagues in [2, 3, 15] adopted approach in which the ratio of rest weight to weight in movement can be altered. This leads to adjustable speed of sound. A reasonable agreement between theory and results was achieved for $Ma < 0.4$. Above 0.4 there are significant discrepancies between theory and simulation. Among fixed value of Prandtl number viscosity was forced to be a function of the variable speed of sound in order to keep the computation stable enough. For this reason the approach is unsuitable for simulation of multiorifice flow.

McNamara [28] presented approach using over-relaxed collision operator. His approach becomes unstable at low viscosity and therefore offers very limited use for application in high Knudsen number regime.

Qian [31] adopted obtained higher order correction to Navier-Stokes dynamics and improved which seems to be different to that of a Burnett equation and therefore relevance of their approach is uncertain.

Different approach was used by Yu or Buick in [9, 47]. They added an attractive force term to the equilibrium distribution function which produced the desired variable speed of sound dependent on the amplitude of the attractive force. The model was verified to be capable of simulating flows up to $Ma \approx 5$ and didn't suffer numerical instabilities due to varied weight of rest distribution function as some of the previous approaches. As authors noted this method introduces artificial viscosity through the additional attractive term and therefore is incapable of accurately capturing throughput.

As argued earlier compressible lattice-Boltzmann models that are looked for must be much more versatile than their incompressible variants. Demand on the Mach number is reaching

value of 2.0 while other requirements are the same as for the incompressible case.

Kataoka in paper [24] showed very interesting idea that is common in the traditional compressible CFD in the limit of small Knudsen number the finite difference form of the lattice-Boltzmann approaches Euler equation as long as a consistent discretization scheme is used. This important result implies that shock-capturing technique should be applied to capture such effects. Based on this he developed several models limiting in compressible Navier-Stokes equations. The drawback of the model is numerical instability when the Mach number reaches 1.0.

Chenghaian in [17] developed the adaptive lattice-Boltzmann model. In this model the structure of lattice velocities varies with the mean flow velocity and the internal energy. This allows the flow to have higher Mach number. Drawback of the method is that unlike the conventional lattice-Boltzmann method where the transported operator is linear in adaptive method transport process is the same as in traditional CFD - non-linear convective streaming. On top of that dimensionless relaxation parameter $\widehat{\tau}$ is fixed which makes used of the method impossible in rarefied flows.

Qu [32] presented approach where Maxwell distribution function is replaced by a spherical function. The function meets all restrictions needed obtain the compressible Navier-Stokes equations in the limit. The circular function is then distributed by Lagrange interpolation to the lattice velocity directions in a similar way as traditional lattice-Boltzmann method. This approach seems to be capable of delivering what is demanded by the multiorifice experiment as the results shows simulations of $Ma = 2.9$. Author conducted only inviscid flow calculations and regarded viscosity effectively as a numerical parameter and there seems to be no other source in the open literature adopting the approach to model high Ma viscous flows.

It seems like Maxwell distribution function or it's modifications may not be the best choice of equilibrium distribution in simulation of compressible flows. In case of thermal compressible flow coefficients $c/\bar{c}$ in the equilibrium distribution function will generate additional terms of the temperature gradients in the process of Chapman-Enskog expansion. This is not the case for isothermal flow where the factor $c/\bar{c}$ cancels out since temperature is considered a constant. Additional temperature gradients don't appear in the macroscopic governing equations. Resulting model fits somewhere between Burnett and Navier-Stokes equations. Navier-Stokes equations are generally considered correct but it is most likely not the case with Burnett model as was shown for instance in [42].

The lowest moments of the distribution function - density, flow velocity and temperature satisfy the conservation equations. For higher order moments of the distribution function the conservation equations are not closed thanks to the higher moments such as stress tensor or heat flux. It is more or less a convention that in Chapman–Enskog successive approximation equations are closed by approximating the fluxes in terms of the lower order moments or their spatial and time derivatives. This procedure successively carries out Euler, Navier–Stokes, Burnett, super-Burnett equations and so forth. Deficiencies naturally appear in more demanding applications such as high Mach or Knudsen number flows. In situation further off the equilibrium state higher order moments become significant for accurate description. The complexity of the Chapman-Enskog calculation increases enormously as the order of approximation increases, yielding highly nonlinear high order partial differential equations. What is even worse than the complexity of

the expansion is that the high order corrections to the Navier–Stokes equations are at least ill-posed.

Chapman-Enskog expansion is used in every place where the need for investigation of limiting hydrodynamic behavior arises. Problem is that from the point of view of mathematical analysis the series is argued to be only asymptotic but not convergent to the correct hydrodynamic behavior. Although this doesn't pose a difficulty when constructing incompressible models that use Chapman-Enskog expansion only up to 2^{nd} order for higher order terms asymptoticity of the series effectively means that terms multiplied by the same order of expansion parameter doesn't yield hydrodynamic behavior of the same magnitude.

In order to make adjustable speed of sound and to deal with it's consequences a more robust to solver like finite volumes or elements might be necessary in order to deal with large gradients. The simulation of compressible flows with strong shock waves is still a challenge even for traditional CFD and significant amount of work is needed in order for lattice-Boltzmann method to be able to mimic the traditional results.

Chapter 6

Numerical Results

6.1 Palabos

All the calculations were performed using Palabos[1] open source software package. The package is primarily intended as solver of incompressible Navier-Stokes equations. The package comes with many small demonstration applications which serve as an excellent starting point for writing user customized problems. There are examples covering multi-component and multi-phase flows, porous media flows, non-Newtonian models and much more. To support users even more there's a lively discussion forum together with instructive manual available at project web page http://www.palabos.org.

Parallelization uses MPI[2] library and scaling properties are excellent both for small and large problems. Historically Palabos is branched from another open source project OpenLB. Interesting insight into decision process behind the implementation of lattice-Boltzmann method can be found in project tech reports on OpenLB web page http://www.openlb.org.

During the development of Palabos accent was placed on object oriented approach. This allowed further extensions of the code which now supports very wide range of both 2D and 3D velocity discretization models and even wider range of boundary conditions. Object oriented programming encapsulates parallel distributed data structures in such way that writing of custom relaxation models or velocity discretization requires no active knowledge of parallel programing concepts which is a huge benefit.

In Listing 6.1 there is the *main* function which every C++ programs contains. On line 2 there's shorthand define statement that specifies the velocity model that will be used in the computation.

Next important section is between lines 9 and 29. Class *RarefiedFlowParam* is an extension of a class distributed with Palabos that calculates and converts domain and dimension related parameters. The class is constructed with all the parameters that are required to setup the computational domain.

On line 32 an instance of *MultiBlock2D* structure is created. The structure represents

[1] Palabos is acronym of Parallel Lattice-Boltzmann Solver

[2] MPI is acronym of Message Passing Interface

lattice where are all the calculations are taking place. The object oriented approach allows to completely cover details of underlying data structures that are indeed very complicated. Among obvious facts that the structure is parallelised and distributed between the computing nodes it also handles communications and sparse domains. The most important parameter passed to the constructor is class *BGKDynamics. BGKDynamics* takes a single parameter - inverse of the relaxation time $1/\hat{\tau}$. *BGKDynamics* can be replaced by any other dynamic class available in Palabos in order to model for instance multi-phase or non-Newtonian fluids is neccesary

On the next two lines we create boundary conditions that are handed over to the functions that are responsible for setup of the domain (*setBoundaryConditions*) and initial conditions (*setInitialConditions*)

The main loop where all the processor time is spend lies between lines 43 and 64. There are some functions handling convergence detection and data writing which are not that important compared to member function of lattice structure *collideAndStream.* This function is responsible for the key part of the calculations. It performs a parallel loop over the whole lattice while streaming and colliding distribution functions.

At the end we clean up the boundary conditions variables.

Listing 6.1: Function *main*

```
1  #define DESCRIPTOR plb::descriptors::D2Q9Descriptor
   using namespace plb;
3  using namespace std;

5  int main(int argc, char* argv[]) {
       plbInit(&argc, &argv);
7      global::directories().setOutputDir("./out/");

9      RarefiedFlowParam<double> flowParam(
           // Knudsen number
11         (double) 0.1,
           // Mach number
13         (double) 0.5,
           // Resolution of lattice
15         (pluint) 200,
           // Width of domain
17         (double) 40,
           // Height of domain
19         (double) 40,
           // Initial lattice density
21         (double) 1.0,
           // Pressure difference
23         (double) 1.0,
           // Diameter of orifices
25         (double) 1.0,
           // Thickness of multiorifice
27         (double) 0.0,
           // Spacing of multiorifice
29         (double) 1.0
       );
31
       MultiBlockLattice2D<double,DESCRIPTOR> lattice(flowParam.getNx(), flowParam.getNy(),
           new BGKdynamics<double, DESCRIPTOR>(flowParam.getOmega()));
33     OnLatticeBoundaryCondition2D<double,DESCRIPTOR>* zouHeBoundaryCondition =
           createZouHeBoundaryCondition2D<double, DESCRIPTOR>();
       OnLatticeBoundaryCondition2D<double,DESCRIPTOR>* inamuroBoundaryCondition =
           createInamuroBoundaryCondition2D<double, DESCRIPTOR>();
35
```

```
    setBoundaryConditions(lattice, *zouHeBoundaryCondition, *inamuroBoundaryCondition,
        flowParam);
    setInitialConditions(lattice, flowParam);

    pluint outiT = 10000;
    pluint dataiT = 10000;
    pluint stopiT = 500000;
    util::ValueTracer<double> valueTracer(flowParam.getDeltaT()/flowParam.getDeltaX(),
        flowParam.getResolution(), 1e-4);
    for (pluint iT = 0; iT <= stopiT; iT++) {
        double avgVelocity = averageOrificeVelocity(lattice, flowParam);
        valueTracer.takeValue(avgVelocity, true);
        if (valueTracer.hasConverged() == true) {
            writeData(lattice, flowParam, iT);
            break;
        }
        if (iT % dataiT == 0) {
            writeData(lattice, flowParam, iT);
        }
        lattice.collideAndStream();
    }

    delete zouHeBoundaryCondition;
    delete inamuroBoundaryCondition;
}
```

In class *initialConditions* defined in Listing 6.2 there is demonstration of interesting programming concept employed in Palabos called the function object. The *operator()* function is overloaded in such way that from a certain perspective function and object becomes indistinguishable. However using object is more beneficial since it allows to store variables and reuse code. Each overloaded version is used to initialize different quantity based on whether the object instance is passed to function setting the velocity or density.

Listing 6.2: Class *initialConditions*

```
template<typename T>
class initialConditions {
public:
    initialConditions(RarefiedFlowParam<T> flowParam_) : flowParam(flowParam_) { }
    // Combined densty and velocity functional
    void operator()(plint iX, plint iY, T& rho, Array<T,2>& u) const {
        rho = analyticDensity(iX, iY);
        u = analyticVelocity(iX, iY);
    }
    // Velocity functional
    void operator()(plint iX, plint iY, Array<T,2>& u) const {
        u = analyticVelocity(iX, iY);
    }
    // Density functional
    T operator()(plint iX, plint iY) const {
        return analyticDensity(iX, iY);
    }
private:
    Array<T,2> analyticVelocity(plint iX, plint iY) const {
        Array<T,2> u;
        u[0] = (T)0.0;
        u[1] = (T)0.0;
        return u;
    }
    T analyticDensity(plint iX, plint iY) const {
        T y = (T)iY / (T)(flowParam.getNy()-1);
        if (y <= 0.5) {
```

```
28            return flowParam.getLatticeRhoBar();
          } else {
30            return flowParam.getLatticeRhoBar() + flowParam.getLatticeRhoDiff();
          }
32      }
      RarefiedFlowParam<T> flowParam;
34  };
```

Function *setInitialConditions* displayed in Listing 6.3 is responsible for preparing the lattice and setting initial values. Function *initializeAtEquilibrium* calls the combined functional form of the *initialConditions* object to set all the distribution function according the equilibrium state determined by the values returned by *initialConditions* object.

Line 3 distributes the *lattice* variable to all computational nodes in cluster environment.

Listing 6.3: Function *setInitialCondition*

```
void setInitialConditions(MultiBlockLattice2D<double,DESCRIPTOR> &lattice,
    RarefiedFlowParam<double> const &flowParam) {
2   initializeAtEquilibrium(lattice, lattice.getBoundingBox(),
        initialConditions<double>(flowParam));
    lattice.initialize();
4   lattice.toggleInternalStatistics(false);
}
```

In Listing 6.4 there is function handling the domain and boundary condition setup. On the first 10 lines it is querying the parameter-storing class *flowParam* about the domain dimensions.

Once the values are obtained it begins to create boxes representing subsets of the lattice where boundary conditions are prescribed. After creation of boxes appropriate boundary condition is prescribed at the nodes residing inside the box. The naming scheme in the source code is consistent with the naming in Figure 6.1

The last two lines finally set values of boundary conditions to the nodes where velocity of pressure boundary condition was prescribed. On other nodes these functions have no effect. The values of boundary conditions are consistent with initial conditions since the same function object is used.

Listing 6.4: Function *setBoundaryCondition*

```
1   void setBoundaryConditions(MultiBlockLattice2D<double,DESCRIPTOR> &lattice,
        OnLatticeBoundaryCondition2D<double,DESCRIPTOR> &domainBoundaryCondition,
        OnLatticeBoundaryCondition2D<double,DESCRIPTOR> &wallBoundaryCondition,
        RarefiedFlowParam<double> const &flowParam) {
      // Width of domain
3     const plint Nx = flowParam.getNx()-1;
      // Height of domain
5     const plint Ny = flowParam.getNy()-1;
      // Diameter of orifice
7     const plint D = flowParam.nCell(flowParam.getOrificeDiameter());
      // Thickness of orifice
9     const plint E = flowParam.nCell(flowParam.getOrificeThickness());
      // Spacing of orifices
11    const plint F = flowParam.nCell(flowParam.getOrificeSpacing());

13    // Bottom boundary gammaB (outlet) left, center and right parts
      Box2D gammaBL(0, 0, 1, (Ny-E)/2);
15    Box2D gammaBC(0, Nx, 0, 0);
      Box2D gammaBR(Nx, Nx, 1, (Ny-E)/2);
17    domainBoundaryCondition.setPressureConditionOnBlockBoundaries(lattice, gammaBL,
          boundary::dirichlet);
```

```
    domainBoundaryCondition.setPressureConditionOnBlockBoundaries(lattice, gammaBC,
        boundary::dirichlet);
    domainBoundaryCondition.setPressureConditionOnBlockBoundaries(lattice, gammaBR,
        boundary::dirichlet);

    // Top boundary gammaT (inlet) left, center and right parts
    Box2D gammaTL(0, 0, (Ny+E)/2+1, Ny-1);
    Box2D gammaTC(0, Nx, Ny, Ny);
    Box2D gammaTR(Nx, Nx, (Ny+E)/2+1, Ny-1);
    domainBoundaryCondition.setPressureConditionOnBlockBoundaries(lattice, gammaTL,
        boundary::dirichlet);
    domainBoundaryCondition.setPressureConditionOnBlockBoundaries(lattice, gammaTC,
        boundary::dirichlet);
    domainBoundaryCondition.setPressureConditionOnBlockBoundaries(lattice, gammaTR,
        boundary::dirichlet);

    // Orifice boundary gammaO  left, center and right parts
    Box2D gammaOL(0, (Nx-F)/2-D, (Ny-E)/2, (Ny+E)/2);
    Box2D gammaOC((Nx-F)/2, (Nx+F)/2, (Ny-E)/2, (Ny+E)/2);
    Box2D gammaOR((Nx+F)/2+D, Nx, (Ny-E)/2, (Ny+E)/2);
    wallBoundaryCondition.setVelocityConditionOnBlockBoundaries(lattice, gammaOL,
        boundary::dirichlet);
    wallBoundaryCondition.setVelocityConditionOnBlockBoundaries(lattice, gammaOC,
        boundary::dirichlet);
    wallBoundaryCondition.setVelocityConditionOnBlockBoundaries(lattice, gammaOR,
        boundary::dirichlet);

    // Set values of boundary conditions
    setBoundaryDensity(lattice, lattice.getBoundingBox(),
        initialConditions<double>(flowParam));
    setBoundaryVelocity(lattice, lattice.getBoundingBox(),
        initialConditions<double>(flowParam));
}
```

Complete source code together with Palabos package version 0.7RC3 are available on the DVD accompanying the thesis. The code can be compiled using latest stable version of gcc or icc compilers at the date of writing the thesis.

6.2 Domain setup

Despite the fact that state of the field of compressible lattice-Boltzmann method is quite unsatisfactory we attempt to predict the distance where orifice stop to influence each other using incompressible lattice-Boltzmann method. However relevance of the results presented in this chapter to the experimental data is at least questionable and direct comparison is impossible.

The main discrepancy between the computational domain and experimental setup is the pressure difference between upstream and downstream chambers. As was stated earlier incompressible lattice-Boltzmann method requires small variations of lattice density to obtain accurate results or even finite. Since scaling parameters of the problem Ma and Kn completely determine the values of time step, space step and relaxation time. It can be clearly seen from the conversion equation for pressure (5.27) that there is no other option on how to accomplish small variations of lattice density than to significantly decrease the driving pressure difference. The effective driving pressure was decreased to $1/1000$ of the experimental value. But apart from pressure the rarefaction approximation of the calculations is believed to be very accurate.

Computations were performed on the domains Ω depicted in Figure 6.1. On the top boundary Γ_T and bottom boundary Γ_B there is Zou's pressure boundary condition prescribed. On the part of the domain representing the orifice Γ_O there is impenetrable wall represented by no-slip Inamuro's boundary condition.

The orifice diameter D was discretized by 200 lattice nodes. The thickness of the orifice was E was 1 row of lattice nodes which can be considered infinitely thin. Overall dimension of the computational domain was $40D \times 40D$. Such large size of the computational domain was forced by Zou's pressure boundary condition and it's property of setting tangential component of velocity to 0. Results are significantly distorted if the duct is placed close to the pressure boundary. Multiorifice spacing F was varied in the interval of $(0.25-5.0)D$ with a step of $0.25D$. Computations were done for three distinct values of Knudsen number $Kn = \{0.01, 0.1, 1.0\}$.

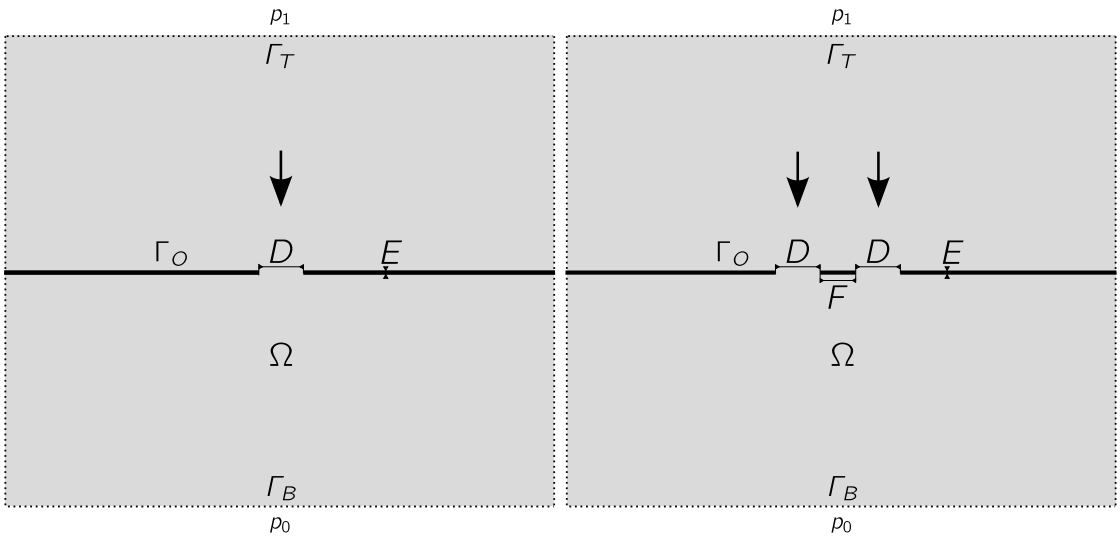

Figure 6.1: Scheme of Orifice and Multiorifice Computational Domain

The calculation was initialized by zero velocity field. Value of initial lattice density is offset by factor of 1 to keep the variations of pressure sufficiently small. Experimental values of pressure are divided by factor of 1000 to maintain incompressible nature of the flow and rescaled values are converted into lattice density by (5.27). Density was initialized as linearly decreasing with the difference between the top and bottom boundary being p_1 since in incompressible flow only difference of pressures has effects on fluid dynamics as long as the variations are kept small.

6.3 Multiorifice Flow Rate

The flow rate in single orifice configuration R_S and flow rate in multiorifice configuration R_M were determined by numeric integration of velocity profiles over cross section of the orifice. Simple trapezoidal rule was used to evaluate integrals. Numeric solutions were obtained on the domains described in the previous chapter.

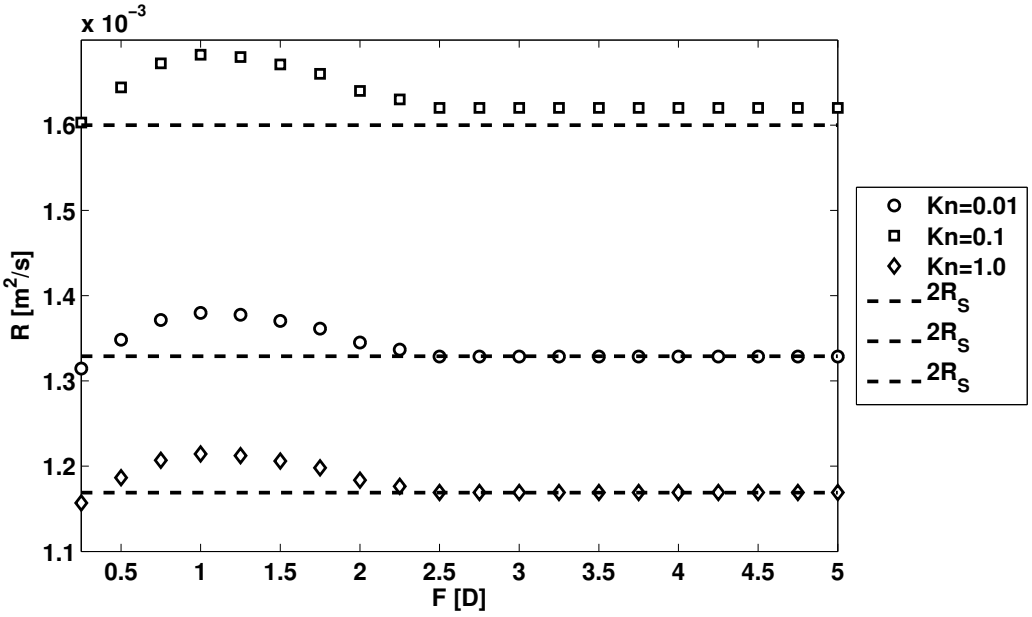

Figure 6.2: Numerical Dependence of Flow Rate on Orifice Spacing

Numerical values of flow rate are plotted in Figure 6.2. The dashed lines represent value of $2R_S$ for respective value of Knudsen number. $2R_S$ is theoretically expected value of flow rate of two single orifices spaced infinitely apart from each other. It can be seen that for larger values of Knudsen number $Kn = \{0.1, 1.0\}$ the theoretical limit is effectively reached up to a precision of several tenths of percent.

In the viscous regime at $Kn = 0.01$ the limit value of flow rate is several percent off the limit value. This can be explained by looking at velocity streamlines in Figure 6.3. In contrary to the previous cases viscosity is large enough to create vortices downstream the orifice. Interaction of vortices is very likely to influence the streamlines even when the orifice is spaced more than $5D$ apart thus modifying flow rate.

From the numerical data it can be clearly identified that the bound where the individual ducts of the multiorifice stops to influence each other is $2.5D$

To get a clearer picture of the character of the flow velocity streamlines in configuration of single orifice and multiorifice with spacings $F = 1D$ and $F = 5D$ with Knudsen number varying in the range specified above are shown in Figures 6.3-6.5. The streamlines visualization applications have some very small but finite value of velocity where the solution of the differential equation stops. This causes some streamlines to begin or end somewhere in the domain although theoretically they should leave it. The results are in agreement with expectations. Flow in lower Knudsen number exhibits tendency to form large eddies and this tendency decreases with decreasing rarefaction.

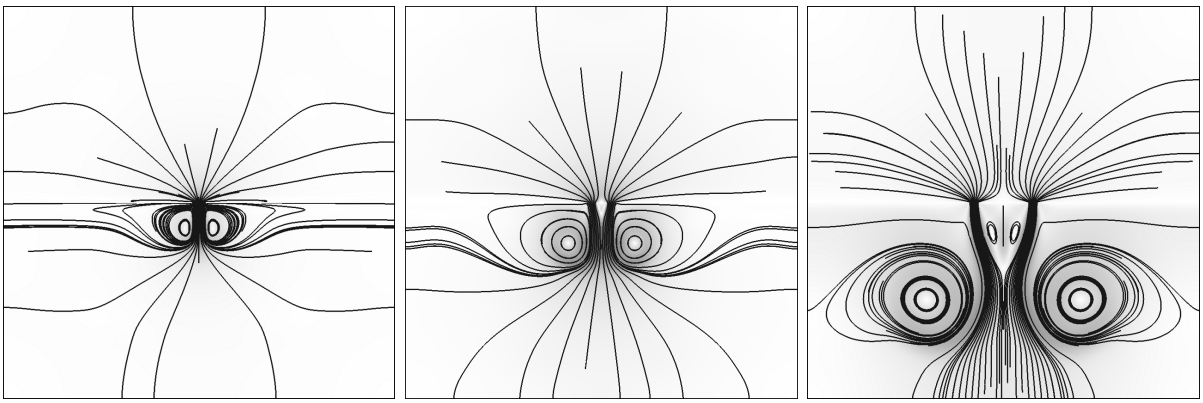

Figure 6.3: Velocity Streamlines at $Kn = 0.01$ in Orifice and Multiorifice with Spacings $F = 1D$ and $F = 5D$ Configurations

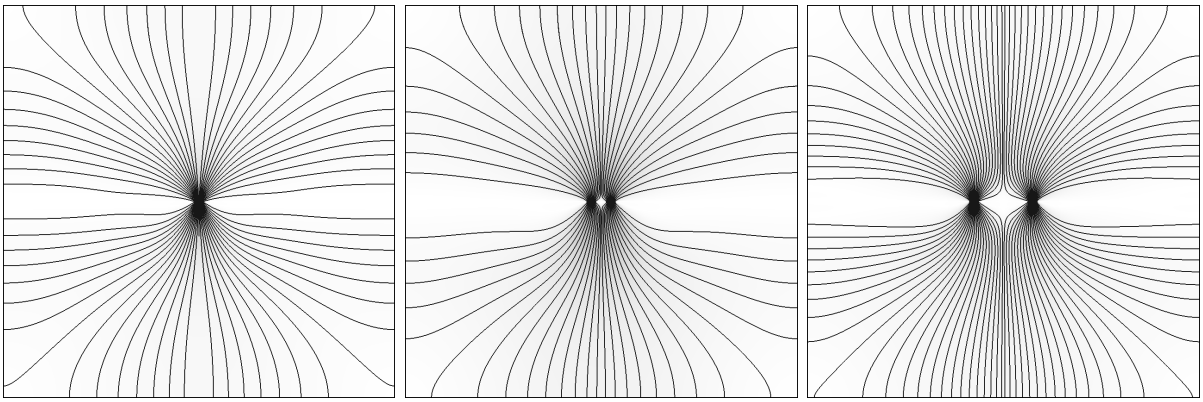

Figure 6.4: Velocity Streamlines at $Kn = 0.1$ in Orifice and Multiorifice with Spacings $F = 1D$ and $F = 5D$ Configurations

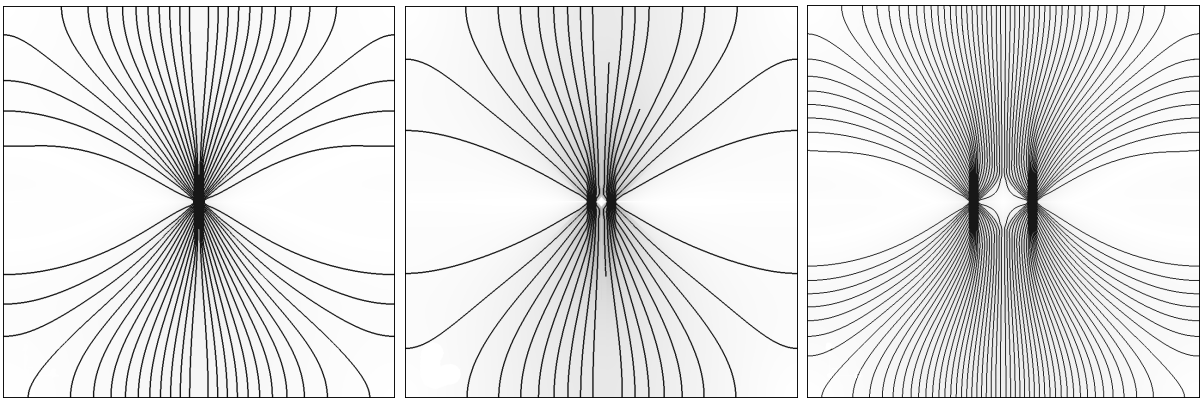

Figure 6.5: Velocity Streamlines at $Kn = 1.0$ in Orifice and Multiorifice with Spacings $F = 1D$ and $F = 5D$ Configurations

6.4 Parallel Scaling

In order to verify parallel scalability of the Palabos code simple numeric scale-up and speed-up tests were performed.

In the speed-up test a problem solving simple pressure driven Poiseuille flow was setup and increasing number of cores was used to find numerical solution. The computational domain consisted of 1000×1000 lattice and 20 000 steps to be performed. The problem was solved with increasing number of used CPUs N_{CPU} up to 64.

The scale-up test maintains constant amount of calculations that needs to be done by one CPU by changing dimension of the problem accordingly. The problem was again simple pressure driven Poiseuille flow. The computational lattice grew linearly with number of cores used to solve the problem as $1000 \times N_{CPU}$ 1000 and number of steps required to evaluate was 20 000.

The scaling results in $MLup/s$ is displayed in Figure 6.6. $MLup/s$ stands for millions of lattice updates per second. It is a standard unit in the field to measure performance of lattice-Boltzmann code.

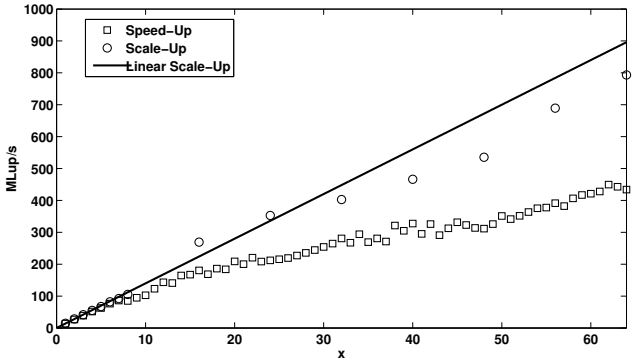

Figure 6.6: Parallel Scale-Up and Speed-Up of Palabos

It can be seen that there's significant drop in efficiency when the size of computational cluster reaches above 8 CPUs. This is caused by the fact that nodes are quad-core dual processor machines and therefore to use more cores the network communication which is several orders of magnitude slower must be used. The linear scale-up slope is determined by extrapolating results achieved on less than 8 computational cores. Slightly misleading results of the scale-up test performing sometimes even better than the linear scalability is caused by the structure of the used cluster. Not all the machines have the same performance. This also explains certain wobbly areas in speed-up test. Generally the data are in qualitative and rough quantitative agreement with scalability test performed on different lattice-Boltzmann solvers running on different machines [**?**].

Chapter 7

Conclusion

After deep analysis we are forced to admit unconditional defeat in our attempt to numerically solve the Boltzmann kinetic equation in the experimental configuration of the multiorifice.

In other rarefied applications numerical solutions were capable of predicting phenomena beyond the Navier-Stokes equation. However the numerical solution is possible only in low Mach number regimes which is not the case in the multiorifice experiment.

There seems to be no available option in the open literature when the Mach number increases and compressibility effects come into play. Source of the problem is nested deep inside of the discretization argumentation chain and it is very hard to point out the weak spot and propose a workaround.

Despite the uncomfortable state of the field we have attempted to numerically predict flow rate and influencing distance of certain configurations of ducts which are unfortunately significantly departed from the original experimental configuration of orifices.

Complete coverage of discretization of Boltzmann kinetic equation known as lattice-Boltzmann method is derived. The scheme of the way loosely followed in the thesis together with key assumptions and hydrodynamic limits can be seen in Figure 7.1.

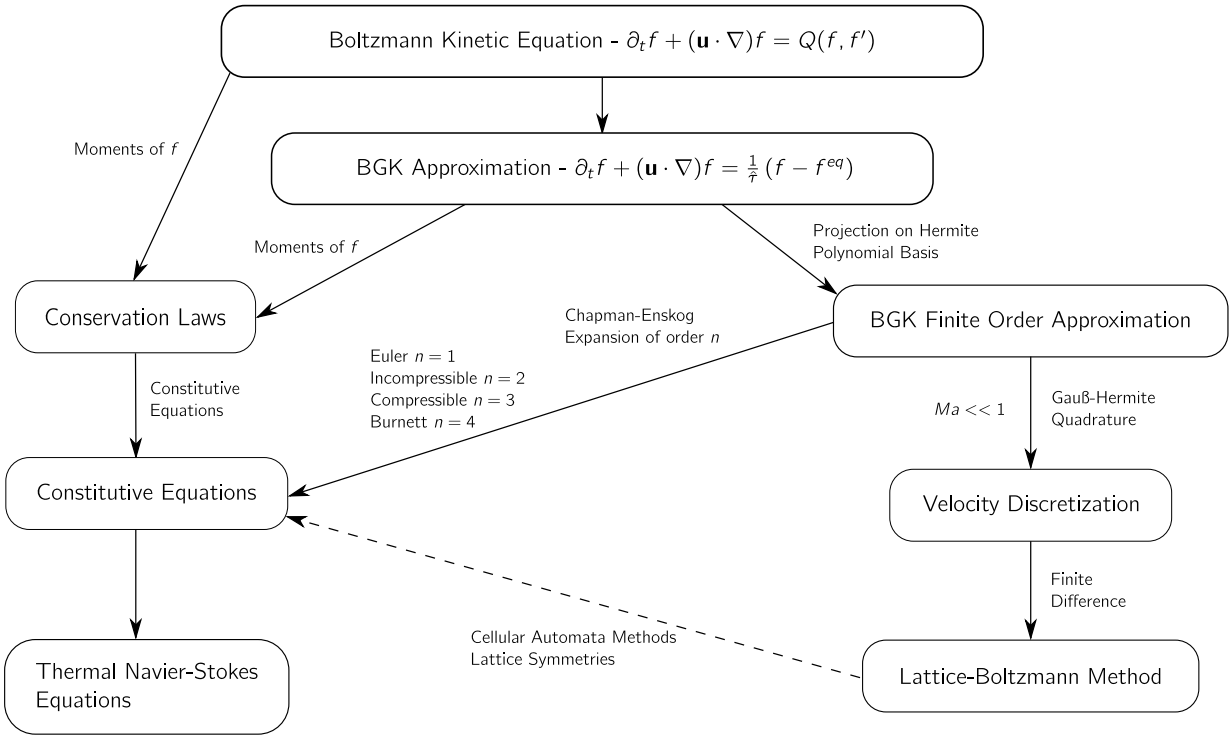

Figure 7.1: Derivation of Numerical Solution and Hydrodynamic Limits

Bibliography

[1] Physical constant, jul 2011.

[2] F. Alexander, H. Chen, S. Chen, and G. Doolen. Lattice boltzmann model for compressible fluids. *Physical Review A 46*, 1992. 5.10

[3] F. Alexander, S. Chen, and J. Sterling. Lattice boltzmann thermohydrodynamics. *Physical Review E 47*, 1993. 5.10

[4] A. S. Berman. Free molecule transmission probabilities. *Journal of Applied Physics 36*, 1965. 2.1

[5] P. L. Bhatnagar, E. P. Gross, and M. Krook. A model for collision processes in gases. i. small amplitude processes in charged and neutral one-component systems. *Physical Review 94*, 1954. 5.1

[6] G. A. Bird. *Molecular Gas Dynamics*. Oxford University Press, Oxford, 1st edition, 1976. 2.1, 3.2

[7] G. A. Bird. *Molecular Gas Dynamics and the Direct Simulation of Fluid Flows*. Oxford University Press, Oxford, 1st edition, 1994. 3.2

[8] J. Boon and J. Rivet. *Lattice Gas Hydrodynamics*. Cambridge University Press, Cambridge, 1st edition, 2001. 3.2

[9] J. Buick and J. Cosgrove. Investigation of a lattice boltzmann model with a variable speed of sound. *Journal of Physics A: Mathematical and General 39*, 2006. 5.10

[10] P. Castulik. Boltzmannovy rovnice a prechod k makroskopickym modelum mechaniky kontinua. Master's thesis, Charles University in Prague, 1998. 4.6

[11] P. Castulik. *Analysis of kinetic equations and their fluid dynamic limits*. PhD thesis, Charles University in Prague, CMLA Ecole Normale Superieure, 2008. 3.2, 4.1, 4.6

[12] C. Cercignani. *The Boltzmann Equation and Its Applications*. Springer-Verlag, Berlin Heidelberg New York, 1st edition, 1988. 3.2, 4.1, 4.2, 4.2, 4.3.2, 4.6

[13] C. Cercignani, R. Illner, and M. Pulvirenti. *The Mathematical Theory of Dilute Gases*. Springer-Verlag, Berlin Heidelberg New York, 1st edition, 1994. 4.1, 4.1, 4.3.2

[14] S. Chapman and Cowling T. *Mathematical Theory of Non-Uniform Gases*. Cambridge University Press, Oxford, 3rd edition, 1970. 4.5

[15] H. Chen, S. Chen, and G. Doolen. Lattice boltzmann model for compressible fluids. *Physica D 47*, 1991. 5.10

[16] S. Chen and J. Sterling. Stability analysis of lattice boltzmann methods. *Journal of Computational Physics 123*, 1996. 5.2, 5.9.1

[17] S. Chenghai and A. Hsu. Multi-level lattice boltzmann model on square lattice for compressible flows. *Computers Fluids 33*, 2004. 5.10

[18] S. Chikatamarla, S. Ansumali, and I. Karlin. Entropic lattice boltzmann models for hydrodynamics in three dimensions. *Physical Review Letters 97*, 2006. 5.9.1

[19] O. Fillipova and D. Hanel. Boundary-fitting and local grid refinement for lbgk models. *International Journal of Modern Physics C 8*, 1998. 5.3

[20] R. W. Hanks and H. L. Weissberg. Slow viscous flow of rarefied gases through short tubes. *Journal of Applied Physics 35*, 1964.

[21] X. He and L. Luo. Lattice boltzmann model for the incompressible navier-stokes equation. *Journal of Statistical Physics 88*, 1997. 5.2

[22] X. He and L. Luo. A priori derivation of the lattice boltzmann equation. *Physical Review E 55*, 1997. 5.2

[23] T. Inamuro, M. Yoshino, and F. Ogino. A non-slip boundary condition for lattice boltzmann simulations. *Physics of Fluids 7*, 1995. 5.7.3

[24] T. Kataoka and M. Tsutahara. Lattice boltzmann model for the compressible navier-stokes equations with flexible specific-heat ratio. *Physical Review E 61*, 2004. 5.10

[25] S. Kim, Pitsch H., and I. Boyd. Slip velocity and knudsen layer in the lattice boltzmann method for microscale flows. *Physical Review E 77*, 2008. 5.8.2

[26] C. Korner, T. Pohl, U. Rude, N. Thurey, and T. Zeiser. *Parallel Lattice Boltzmann Methods for CFD Applications*. Springer, 2006.

[27] J. Latt. *Hydrodynamic Limit of Lattice Boltzmann Equations*. PhD thesis, University of Geneva, 2007. 5.8.1

[28] G. McNamara and B. Alder. Analysis of the lattice boltzmann hydrodynamics. *Physica A 194*, 1993. 5.10

[29] X. Nie, G. Doolen, and Chen S. Lattice-boltzmann simulations of fluid flows in mems. *Journal of Statistical Physics 107*, 2002. 5.8.2

[30] D. Noble, Chen S., J. Georgiadis, and R. Buckius. A consistent hydrodynamic boundary condition for the lattice boltzmann method. *Physics of Fluids 7*, 1995. 5.7.2

[31] Y. Qian and S. Orszag. Lattice bgk models for the navier-stokes equation: Nonlinear deviation in compressible regimes. *Europhysics Letters 21*, 1993. 5.10

[32] K. Qu, C. Shu, and Y. Chew. Alternative method to construct equilibrium distribution functions in lattice-boltzmann method simulation of inviscid compressible flows at high mach number. *Physical Review E 75*, 2007. 5.10

[33] M. Renwei, Li-Shi L., and W. Shyya. An accurate curved boundary treatment in the lattice boltzmann method. *Journal of Computational Physics 155*, 1999. 5.7.4

[34] D. Rothman and Zaleski S. *Lattice-Gas Cellular Automata Simple models of complex hydrodynamics*. Cambridge University Press, Cambridge, 1st edition, 1999. 3.2

[35] L. Saint-Raymond. *Hydrodynamic Limits of the Boltzmann Equation, Lecture Notes in Mathematics*, volume 1971. Springer, Berlin Heidelberg New York, 1st edition, 2009. 3.2, 4.6

[36] X. Shan and X. He. Discretization of the velocity space in the solution of the boltzmann equation. *Physical Review Letters 80*, 1998. 5.2

[37] X. Shan and X. He. Lattice boltzmann method for fluid flows. *Annual Review of Fluid Mechanics 30*, 1998. 5.7.1

[38] X. Shan, X. Yuan, and H. Chen. Kinetic theory representation of hydrodynamics: a way beyond the navier-stokes equation. *Journal of Fluid Mechanics 550*, 2006. 5.9.2

[39] F. Sharipov. Numerical simulation of rarefied gas flow through a thin orifice. *Journal of Fluid Mechanics 518*, 2004. 5.9.2

[40] F. Sharipov, O. Sazhin, S. Varoutis, and D. Velougeorgis. Rarefied gas flow through short tubes into vacuum. *Journal of Vacuum Science and Technology A 26*, 2008. 5.9.2

[41] P. Skordos. Initial and boundary conditions for the lattice boltzmann method. *Physical Review E 48*, 1993. 5.7

[42] H. Struchtrup. Failures of the burnett and super-burnett equations in steady state processes. *Continuum Mechanics and Thermodynamics 17*, 2005. 5.10

[43] S. Succi. *Lattice Boltzmann Equation for Fluid Dynamics and Beyond*. Oxford University Press, 2001. 5.8.2

[44] S. Succi. Lattice boltzmann method at finite knudsen numbers. *Europhysics Letters 77*, 2005. 5.8.2

[45] E. Viggen. The lattice boltzmann method with applications in acoustics. Master's thesis, Norwegian University of Science and Technology, 2009. 5.8.1, 5.8.2

[46] D. A. Wolf-Gladrow. *Lattice-Gas Cellular Automata and Lattice Boltzmann Models, Lecture Notes in Mathematics*, volume 1925. Springer, Berlin Heidelberg New York, 1st edition, 2000. 3.2

[47] H. Yu and Z. Kaihua. Lattice boltzmann method for compressible flows with high mach numbers. *Physical Review E 61*, 2000. 5.10

[48] Y. Zhang. Lattice boltzmann simulation of rarefied gas flows in microchannels. *Physical Review E 71*, 2005. 2.2, 5.8.2

[49] Q. Zou and X. He. On pressure and velocity flow boundary conditions and bounceback for the lattice boltzmann bgk model. *Physics of Fluids 9*, 1997. 5.7.2